



Spectral signature of nonlinear effects in semiconductor optical amplifiers

ANDREJ MARCULESCU,^{1,2,*} SEÁN Ó DÚILL,^{1,3} CHRISTIAN KOOS,¹
WOLFGANG FREUDE,¹ AND JUERG LEUTHOLD^{1,2}

¹*Institute of Photonics and Quantum Electronics (IPQ), Karlsruhe Institute of Technology, Karlsruhe, Germany*

²*Now with: Institute of Electromagnetic Fields (IEF), ETH Zurich, Zurich, Switzerland*

³*Now with: School of Electronic Engineering, Dublin City University, Dublin 9, Ireland*

**andrej@marculescu.de*

Abstract: Optical spectra of signals at the output of semiconductor optical amplifiers (SOA) provide useful insight into amplifier nonlinearities. In this work, we determine the parameters of an analytical SOA model with a pump-probe experiment by evaluating the measured spectra of the pump and probe pulses at the SOA output. The analytical lumped SOA model considers carrier depletion, carrier recovery, spectral hole burning, two-photon absorption, and we include an additional effect termed ‘two-photon induced free-carrier absorption’, that is responsible for creating an identifiable blue-shifted component in the spectra. We are able to relate the underlying physical nonlinear effects to the spectral peculiarities of the output pump and probe spectra, and give guidelines for the exploitation of these nonlinear effects for optical signal processing. In addition, with a much-simplified SOA model and by replacing the pump pulse with modulated data we show that the output spectrum is altered in a manner consistent with phase patterning effects.

©2017 Optical Society of America

OCIS codes: (250.5980) Semiconductor optical amplifiers; (190.4360) Nonlinear optics, devices.

References and links

1. B. Filion, W. C. Ng, A. T. Nguyen, L. A. Rusch, and S. Larochelle, “Wideband wavelength conversion of 16 Gbaud 16-QAM and 5 Gbaud 64-QAM signals in a semiconductor optical amplifier,” *Opt. Express* **21**(17), 19825–19833 (2013).
2. S. T. Naimi, S. P. Ó. Duill, and L. P. Barry, “All optical wavelength conversion of Nyquist-WDM superchannels using FWM in SOAs,” *J. Lightwave Technol.* **33**(19), 3959–3967 (2015).
3. B. Filion, L. Jiachuan, A. T. Nguyen, X. Zhang, S. LaRochelle, and L. A. Rusch, “Semiconductor optical amplifier-based wavelength conversion of Nyquist-16QAM for flex-grid optical networks,” *J. Lightwave Technol.* **34**(11), 2724–2729 (2016).
4. A. P. Anthur, R. Zhou, S. O’Duill, A. J. Walsh, E. Martin, D. Venkitesh, and L. P. Barry, “Polarization insensitive all-optical wavelength conversion of polarization multiplexed signals using co-polarized pumps,” *Opt. Express* **24**(11), 11749–11761 (2016).
5. A. P. Anthur, R. T. Watts, K. Shi, J. O. Carroll, D. Venkitesh, and L. P. Barry, “Dual correlated pumping scheme for phase noise preservation in all-optical wavelength conversion,” *Opt. Express* **21**(13), 15568–15579 (2013).
6. G. Contestabile, “Wavelength conversion of PAM signals by XGM in SOAs,” in *Asia Communications and Photonics Conference*, OSA Technical Digest (Optical Society of America, 2016), paper AF4H.4.
7. C. T. Hultgren and E. P. Ippen, “Ultrafast refractive index dynamics in AlGaAs diode laser amplifiers,” *Appl. Phys. Lett.* **59**(6), 635–637 (1991).
8. T. Vallaitis, C. Koos, R. Bonk, W. Freude, M. Laemmlin, C. Meuer, D. Bimberg, and J. Leuthold, “Slow and fast dynamics of gain and phase in a quantum dot semiconductor optical amplifier,” *Opt. Express* **16**(1), 170–178 (2008).
9. C. Dorrer and I. Kang, “Simultaneous temporal characterization of telecommunication optical pulses and modulators by use of spectrograms,” *Opt. Lett.* **27**(15), 1315–1317 (2002).
10. M. G. Kane, I. Glesk, J. P. Sokoloff, and P. R. Prucnal, “Asymmetric optical loop mirror: analysis of an all-optical switch,” *Appl. Opt.* **33**(29), 6833–6842 (1994).
11. J. Leuthold, P. A. Besse, J. Eckner, E. Gamper, M. Dulk, and H. Melchior, “All-optical space switches with gain and principally ideal extinction ratios,” *IEEE J. Quantum Electron.* **34**(4), 622–633 (1998).
12. C. H. Henry, “Theory of the linewidth of semiconductor lasers,” *IEEE J. Quantum Electron.* **18**(2), 259–264 (1982).
13. J. Wang, A. Maitra, C. G. Poulton, W. Freude, and J. Leuthold, “Temporal dynamics of the alpha factor in semiconductor optical amplifiers,” *J. Lightwave Technol.* **25**(3), 891–900 (2007).

14. M. Willatzen, A. Uskov, J. Mørk, H. Olesen, B. Tromborg, and A.-P. Jauho, "Nonlinear gain suppression in semiconductor lasers due to carrier heating," *IEEE Photonics Technol. Lett.* **3**(7), 606–609 (1991).
15. J. Mørk and A. Mecozzi, "Response function for gain and refractive index dynamics in active semiconductor waveguides," *Appl. Phys. Lett.* **65**(14), 1736–1738 (1994).
16. S. Krishnamurthy, Z. G. Yu, L. P. Gonzalez, and S. Guha, "Temperature and wavelength-dependent two-photon and free-carrier absorption in GaAs, InP, GaInAs, and InAsP," *J. Appl. Phys.* **109**(3), 033102 (2011).
17. P. Y. Yu and M. Cardona, *Fundamentals of Semiconductors* (Springer, 2010), Ch. 5.
18. E. M. Conwell and M. O. Vassell, "High-field distribution function in GaAs," *IEEE Trans. Electron Dev.* **13**(1), 22–26 (1966).
19. G. Klimeck, R. C. Bowen, T. B. Boykin, and T. A. Cwik, "sp³s* tight-binding parameters for transport simulations in compound semiconductors," *Superlattices Microstruct.* **27**(5–6), 519–524 (2000).
20. P. Lunnemann, S. Ek, K. Yvind, R. Piron, and J. Mørk, "Nonlinear carrier dynamics in a quantum dash optical amplifier," *New J. Phys.* **14**(1), 013042 (2012).
21. J. Mørk and A. Mecozzi, "Theory of the ultrafast optical response of active semiconductor waveguides," *J. Opt. Soc. Am. B* **13**(8), 1803–1816 (1996).
22. G. P. Agrawal and N. A. Olsson, "Self-phase modulation and spectral broadening of optical pulses in semiconductor laser amplifiers," *IEEE J. Quantum Electron.* **25**(11), 2297–2306 (1989).
23. A. Mecozzi and J. Mørk, "Theory of heterodyne pump-probe experiments with femtosecond pulses," *J. Opt. Soc. Am. B* **13**(11), 2437–2452 (1996).
24. A. Mecozzi and J. Mørk, "Saturation induced by picosecond pulses in semiconductor optical amplifiers," *J. Opt. Soc. Am. B* **14**(4), 761–770 (1997).
25. M. Premaratne, D. Nestic, and G. P. Agrawal, "Pulse amplification and gain recovery in semiconductor optical amplifiers," *J. Lightwave Technol.* **26**(12), 1653–1660 (2008).
26. I. D. Rukhlenko, M. Premaratne, and G. P. Agrawal, "Nonlinear Silicon Photonics: Analytical Tools," *IEEE J. Sel. Top. Quantum Electron.* **16**(26), 200–215 (2010).
27. J. E. Carroll, J. Whiteaway, and D. Plumb, *Distributed Feedback Semiconductor Lasers* (Institute of Electrical Engineers, 1998).
28. J. M. Tang and K. A. Shore, "Strong picosecond optical pulse propagation in semiconductor optical amplifiers at transparency," *IEEE J. Quantum Electron.* **34**(7), 1263–1269 (1998).
29. A. Mecozzi and J. Mørk, "Saturation effects in nondegenerate four-wave mixing between short optical pulses in semiconductor laser amplifiers," *IEEE J. Sel. Top. Quantum Electron.* **3**(5), 1190–1207 (1997).
30. M. Sheik-Bahae and E. W. Van Stryland, "Optical nonlinearities in the transparency region of bulk semiconductors" in *Nonlinear Optics in Semiconductors I*, E. Garmire and A. Kost, eds. (Academic, 1999).
31. D. Hutchings and E. Van Stryland, "Nondegenerate two-photon absorption in zinc blende semiconductors," *J. Opt. Soc. Am. B* **9**(11), 2065–2074 (1992).
32. B. Olson, M. Gehlsen, and T. Boggess, "Nondegenerate two-photon absorption in GaSb," *Opt. Commun.* **304**, 54–57 (2013).
33. C. H. Henry, R. A. Logan, and K. A. Bertness, "Spectral dependence of the change in refractive index due to carrier injection in GaAs lasers," *J. Appl. Phys.* **52**(7), 4457–4461 (1981).
34. R. Giller, R. J. Manning, and D. Cotter, "Gain and phase recovery of optically excited semiconductor optical amplifiers," *IEEE Photonics Technol. Lett.* **18**(9), 1061–1063 (2006).
35. I. Kang and C. Dorrer, "Measurements of gain and phase dynamics of a semiconductor optical amplifier using spectrograms," in *Optical Fiber Communication Conference*, OSA Technical Digest Series (Optical Society of America, OFC 2004), paper MF43.
36. R. S. Grant and W. Sibbett, "Observations of ultrafast nonlinear refraction in an InGaAsP optical amplifier," *Appl. Phys. Lett.* **58**(11), 1119–1121 (1991).
37. Y. Ueno, S. Nakamura, and K. Tajima, "Nonlinear phase shifts induced by semiconductor optical amplifiers with control pulses at repetition frequencies in the 40–160-GHz range for use in ultrahigh-speed all-optical signal processing," *J. Opt. Soc. Am. B* **19**(11), 2573–2589 (2002).
38. O. Raz, J. Herrera, and H. J. Dorren, "Enhanced 40 and 80 Gb/s wavelength conversion using a rectangular shaped optical filter for both red and blue spectral slicing," *Opt. Express* **17**(3), 1184–1193 (2009).
39. J. Leuthold, R. Ryf, D. N. Maywar, S. Cabot, J. Jaques, and S. S. Patel, "Nonblocking all-optical cross connect based on regenerative all-optical wavelength converter in a transparent demonstration over 42 nodes and 16800 km," *J. Lightwave Technol.* **21**(11), 2863–2870 (2003).
40. M. L. Nielsen, B. Lavigne, and B. Dagens, "Polarity-preserving SOA-based wavelength conversion at 40 Gbit/s using bandpass filtering," *Electron. Lett.* **39**(18), 1334–1335 (2003).
41. Y. Liu, E. Tangdiongga, Z. Li, H. de Waardt, A. M. J. Koonen, G. D. Khoe, X. Shu, I. Bennion, and H. J. S. Dorren, "Error-free 320-Gb/s all-optical wavelength conversion using a single semiconductor optical amplifier," *J. Lightwave Technol.* **25**(1), 103–108 (2007).
42. J. Leuthold, D. M. Marom, S. Cabot, J. J. Jaques, R. Ryf, and C. R. Giles, "All-optical wavelength conversion using a pulse reformatting optical filter," *J. Lightwave Technol.* **22**(1), 186–192 (2004).
43. J. Wang, A. Marculescu, J. Li, P. Vorreau, S. Tzadok, S. Ben Ezra, S. Tsadka, W. Freude, and J. Leuthold, "Pattern effect removal technique for semiconductor-optical-amplifier-based wavelength conversion," *IEEE Photonics Technol. Lett.* **19**(24), 1955–1957 (2007).
44. X. Wei and J. Leuthold, "Relation between vestigial-sideband filtering and $\pi/2$ progressive phase shift," *Opt. Lett.* **29**(14), 1599–1601 (2004).

45. J. Wang, A. Marculescu, J. Li, Z. Zhang, W. Freude, and J. Leuthold, "All-optical vestigial-sideband signal generation and pattern effect mitigation with an SOA based red-shift optical filter wavelength converter," in *Proc. 33rd European Conference on Optical Communication, (ECOC 2008)*, paper We.2.C.6.
46. A. Marculescu, S. Sygletos, J. Li, D. Karki, D. Hillerkuß, S. Ben-Ezra, S. Tsadka, W. Freude, and J. Leuthold, "RZ to CSRZ Format and Wavelength Conversion with Regenerative Properties," in *Optical Fiber Communication Conference, OSA Technical Digest Series (Optical Society of America, OFC 2009)*, paper OThS1.
47. M. L. Nielsen and J. Mørk, "Increasing the modulation bandwidth of semiconductor-optical-amplifier-based switches by using optical filtering," *J. Opt. Soc. Am. B* **21**(9), 1606–1619 (2004).

1. Introduction

Semiconductor optical amplifiers (SOA) are key components for both, linear amplification in access networks, and nonlinear ultrafast all-optical signal processing such as wavelength conversion, or all-optical logic gating. Cross gain modulation (XGM) and cross phase modulation (XPM) are the techniques of choice for signals with intensity modulation; the recent deployment of advanced modulation formats such as quadrature phase shift keying (QPSK), 16-state quadrature amplitude modulation (16-QAM) and 64-QAM has motivated studies into using four-wave mixing (FWM) effects in SOAs to perform wavelength conversion [1–4]. The power penalty for employing FWM in SOAs can be well below 1 dB [5]. The information carrying capacity of intensity-modulated signals can be doubled by increasing the number of amplitude levels to four by using four-level pulse amplitude modulation (PAM-4), and XGM has been studied to perform wavelength conversion of PAM-4 signals in SOAs [6]. Given the huge interest in all-optical signal processing using SOAs and the potential benefits arising thereof, a proper design of nonlinear SOAs requires models that allow to derive the slow and ultrafast gain and refractive index dynamics, where a multitude of nonlinear effects act on different timescales.

There are several methods to characterize nonlinear effects in an SOA. Unfortunately, all of them are experimentally quite demanding: Pump-probe sampling techniques together with heterodyne detection allow phase and amplitude resolutions that are only limited by the full width at half maximum (FWHM) of the pump pulse [7,8]. Alternatively, indirect methods such as frequency-resolved electro-absorption gating (FREAG) [9] can be employed. The temporal resolution is limited by the rise time of the optical gate, and computationally expensive algorithms are required to resolve the gain and index dynamics. In addition, various other techniques, where devices are positioned in an interferometer and the amplitude and phase response are derived from the interferometer pattern, have been elaborated [10,11].

In this paper, we derive the temporal gain and phase dynamics of SOAs operated in the nonlinear regime from measured time-averaged optical spectra at the SOA output. We are including the following nonlinear effects in SOAs [12–15]: bandfilling that treats both carrier depletion and recovery, carrier heating, spectral hole burning, two-photon absorption, and we introduce an effect termed two-photon absorption induced free-carrier absorption (FCA_{TPA}) [16] that accounts for the large blue-shifted component especially in the probe spectrum. The measured output spectra reflect the temporal dependence of the output pulse and continuous wave (CW) probe that undergoes cross-gain (and cross-phase) modulation. By fitting a closed-form model to the measured spectra, we can separate the gain and refractive index dynamics of the SOA as well as extracting physically meaningful model parameters. We explain how the nonlinear processes have their own unique spectral signatures; we pay special attention to the blue-shifted components of the probe spectrum. We identify that a distinctive feature in the blue-shifted sideband of the probe spectrum indicates the occurrence of the FCA_{TPA} process. This blue-shifted component is recognizable by mere inspection of the probe spectrum and is exploitable for ultrafast all-optical signal processing purposes. Only modest measurement apparatus is required comprising of a picosecond pump laser source, a CW probe laser, and an optical spectrum analyzer (OSA); this equipment is standard within optics and photonics research laboratories. Neither high-speed electronic modulation, nor detection, sampling, or all-optical probing with femtosecond pulses is required. Moreover, in a wavelength conversion experiment with a data signal and a probe light, the probe spectrum after the SOA provides information about phase patterning effects.

The paper is organized as follows: In Section 2, we derive the nonlinear model of the gain and refractive index dynamics. These dynamics are formulated in terms of differential equations with boundary or initial conditions that are known to have unique solutions. In the following Section 3, we compare the model to the measured spectra and extract the model parameters, which describe the relevant nonlinear dynamic processes within the SOA. In Section 4, we use this knowledge to design filters for all-optical wavelength conversion (AOWC). Finally, in Section 5, we show that patterning effects in AOWC can be predicted from a signature analysis of the converted signal spectrum.

2. Model of SOA gain and refractive index dynamics

The SOA model in this work relates to a typical experimental condition. We evaluate the SOA gain and refractive index dynamics by the mutual influence of a strong 2.8 ps wide input pump pulse and a weak continuous wave (CW) input probe light. Pump and probe wavelengths are closely neighbored within the gain bandwidth of the SOA. If the pump saturates the SOA gain, the local charge carrier density reduces, which in turn changes the temporal evolution of the pump signal, Fig. 1(a), and the probe light, Fig. 1(b), at the SOA's output. Changes of the modal gain g and of the refractive index n with respect to the carrier density N are interrelated by the Kramers-Kronig relations, which can be approximated by the linewidth enhancement factor (Henry factor, α -factor) [12]

$$\alpha = -2k_0 \frac{\partial n / \partial N}{\partial g / \partial N} \approx -2k_0 \frac{\Delta n}{\Delta g}, \quad k_0 = \frac{\omega_0}{c}, \quad (1)$$

where ω_0 stands for the closely neighbored pump signal (subscript S) and probe (subscript \times) angular frequencies $\omega_s \approx \omega_x \approx \omega_0$, and c is the vacuum speed of light. The changes in refractive index and modal gain are denoted by Δn and Δg , respectively.

2.1. General description

Before explaining the details of the model, we review the most relevant gain dynamics and gain-saturating processes in SOAs which occur on vastly different time scales [13]. Different α -factors can be attributed to these processes. For simplicity, carrier diffusion along the SOA is neglected.

(i) *Band filling (BF)*. BF relates to the total number of carriers within the energy bands of the SOA. The dynamics comprises carrier depletion (CD) followed by subsequent carrier recovery (CR). The first effect is fast, because stimulated recombination is virtually instantaneous on the timescale of the pulse duration. Carrier depletion increases the refractive index. The recovery, which implies refilling of electrons and holes back to the concentration of the small-signal gain, takes place on a timescale of about 100 ps, which is much longer than the pump pulse duration. The α -factor associated with BF is denoted by α_{BF} . In some publications, the symbol α_N is used instead.

(ii) *Spectral hole burning (SHB)*. The pump signal depletes the carriers virtually instantaneously at the pump photon energy so that a "hole" is burned into the gain spectrum. The empty states of the band are refilled through carrier-carrier scattering on a time scale of about 100 fs [14]. The change in gain due to SHB has a symmetric spectral profile around the center frequency ω_s of the pump and does not change the refractive index [15]. Because the probe frequency ω_x is close to ω_s , the spectral symmetry applies also to the probe, and we therefore neglect the probe's SHB contribution to the refractive index. Consequently, the associated α_{SHB} factor is assumed to be zero.

(iii) *Carrier heating (CH)*. If carrier equilibrium inside a band is destroyed by rapid processes, the instantaneous carrier occupation probability cannot be described anymore

with a Fermi function. However, after refilling the unoccupied states left by SHB, the carrier occupation probability follows again a Fermi distribution with an effective “hot” carrier temperature larger than the lattice temperature. The process is named carrier heating. By heating the carrier distribution, the gain decreases [14] and the refractive index increases. Subsequently, the hot carriers cool down (carrier cooling, CC), and the gain relaxes back on a timescale of up to a picosecond (carrier heating relaxation time) [14]. The gain changes lead to refractive index changes, and the associated α -factor is denoted by α_{CH} .

(iv) *Two-photon absorption (TPA) and TPA-induced free-carrier absorption (FCA_{TPA}).* Two photons with the same or with different energies can be absorbed simultaneously. This process is rather unlikely, and therefore large powers (large photon numbers) are needed for this effect to be significant. Electrons are lifted virtually instantaneously from the valence band (VB) to the conduction band (CB). The TPA process can occur with simultaneous absorption of two pump photons (degenerate TPA), or with the simultaneous absorption of a pump and of a probe light photon (nondegenerate TPA). For nondegenerate TPA, the polarizations of the optical fields play an important role, such that even for a weak probe light the corresponding TPA absorption coefficient can become twice as large as for degenerate TPA. Although a nondegenerate TPA-process may enhance the absorption coefficient for the probe light, the additional number of photoexcited electrons is too small for a significant change of the refractive index if the probe light is sufficiently weak. The associated increased optical loss with degenerate and nondegenerate TPA and the increased number of carriers lead to an instantaneous decrease of the refractive index [7]. The α -factor associated with the TPA process is thus negative and will be denoted by α_{TPA} . Carriers generated via TPA can become available for free-carrier absorption (FCA), we denote this process FCA_{TPA} , and explain it as follows: For sufficiently strong pulses and semiconductors of suitably small bandgap, two-photon absorption generates an appreciable population of photoexcited electrons in the Γ -valley of the lowest conduction band (CB) [16]. If this Γ -valley is filled or if the sum energy of the two photons is large enough, lower unoccupied states in side-valleys [17], e.g., in the X-valley, can be filled. In this case, however, an additional phonon has to deliver the required difference in crystal momentum. This is also true if electrons in Γ -valley states are to be scattered into the same-energy X-valley states [17,18]. The transfer of the photoexcited electrons from the Γ -valley to the satellite X-valley needs a finite amount of time τ_0 [18], usually termed intervalley scattering time. Since the bottom of the X-valley lies close [19] to the next higher CB, electrons which reached this side-valley can absorb one more photon (direct absorption) and make a momentum-conserving upwards transition to the next higher conduction band without the assistance of a phonon. This direct, TPA-induced free-carrier absorption (FCA_{TPA}) has been demonstrated [16] for the binary compounds GaAs and InP. Similar to TPA, TPA-induced FCA increases the optical loss so that the refractive index decreases [20]. However, this refractive index change occurs delayed by the intervalley scattering time τ_0 . An instantaneous FCA_{TPA} -effect requires a simultaneous absorption of a photon to conserve both, energy and momentum, and can be neglected [16]. A pictorial explanation of both instantaneous and delayed FCA_{TPA} -processes is given in Appendix A. Intervalley scattering effect may well have other significance for SOAs. In previous work from our group [13] intervalley scattering would explain the required higher-order correction term applied to the carrier density rate equation in [13], Eq. (13), whereby carrier leakage at high carrier energies was necessary to get a good fitting with experiments.

The aforementioned effects can be identified when looking at the evolution of the input pump signal (subscript S) and the input CW probe light (subscript \times) inside the SOA. We assume single-mode propagation and represent the waveguide mode by a plane wave with an

effective propagation constant $k_0 n_0$ and an effective refractive index n_0 . The fields depend on the coordinates z (position) and t (time), and are represented by the square root of the respective powers. Denoting the powers by $P_{\gamma S,x}(z,t)$ and the phases by $\varphi_{\gamma S,x}(z,t)$ we write the normalized root-mean-squared (RMS) electric fields as

$$E_{\gamma S,x}(z,t) = \sqrt{P_{\gamma S,x}(z,t)} \exp[j\varphi_{\gamma S,x}(z,t)] \exp[j(\omega_{S,x}t - k_0 n_0 z)]. \quad (2)$$

The SOA length is denoted by L . We attach the superscript in (out) to the functions of time at the SOA input (output) at position $z = 0$ ($z = L$). Then the input and output normalized RMS fields are given by

$$E_{\gamma S,x}^{\text{in}}(t) = \sqrt{P_{\gamma S,x}^{\text{in}}(t)} \exp[j\varphi_{\gamma S,x}^{\text{in}}(t)] \exp(j\omega_{S,x}t) \quad (3)$$

and

$$E_{\gamma S,x}^{\text{out}}(t) = \sqrt{P_{\gamma S,x}^{\text{out}}(t)} \exp[j\varphi_{\gamma S,x}^{\text{out}}(t)] \exp[j(\omega_{S,x}t - k_0 n_0 L)], \quad (4)$$

respectively. We further assume that the probe light power is much smaller than the pump light power so that four-wave mixing between pump and probe remains insignificant. In this case coherent interaction is excluded so that the phase relation between pump and probe is unimportant, and the assignments $\varphi_{\gamma S,x}^{\text{in}}(t) = 0$ for both the pump and the probe are justified. Pump wave and probe wave (influenced by the pump) have complex valued envelopes with a typical width of 2.8 ps,

$$\mathcal{E}_{\gamma S,x}(z,t) = \sqrt{P_{\gamma S,x}(z,t)} \exp[j\varphi_{\gamma S,x}(z,t)]. \quad (5)$$

When pump and probe propagate simultaneously through the amplifier, the response of the nonlinear medium depends on the powers $P_{\gamma S}(z,t)$ and $P_{\gamma x}(z,t)$ of both co-propagating fields. This response can be described by a complex refractive index $\underline{n}_{\gamma S,x}(z,t)$, which is split in a coordinate-independent part n_0, g_0 and a coordinate-dependent contribution $\Delta n_{\gamma S,x}(z,t)$, $\Delta g_{\gamma S,x}(z,t)$. Real and imaginary parts define the refractive index $n_{\gamma S,x}(z,t)$ and the modal gain $g_{\gamma S,x}(z,t)$, respectively. As $\omega_S \approx \omega_x \approx \omega_0$ holds, we write

$$\begin{aligned} \Delta \underline{n}_{\gamma S,x}(z,t) &= \underline{n}_{\gamma S,x}(z,t) - n_0 = \Delta n_{\gamma S,x}(z,t) + \frac{j}{2k_0} g_{\gamma S,x}(z,t), \\ g_{\gamma S,x}(z,t) &= g_0 + \Delta g_{\gamma S,x}(z,t). \end{aligned} \quad (6)$$

While the dominant coordinate-independent part is virtually the same for both signals, the coordinate-dependent contributions $\Delta n_{\gamma S}(z,t)$ and $\Delta n_{\gamma x}(z,t)$ are in general different because the SOA nonlinearity couples the two optical fields through a nondegenerate TPA process. We also assume that both signals propagate with the same group velocity v_g , have a negligible group-velocity dispersion [21], and the wavelengths of both pump and probe are close to the wavelength of the SOA gain peak so that SOA gain-dispersion can be ignored, i.e., $\partial g_{\gamma S,x} / \partial \omega_{S,x} = 0$. For simplicity, throughout this paper we neglect the internal loss coefficient α_{int} . In the slowly-varying envelope approximation [22], the complex-valued envelope function $\mathcal{E}_{\gamma S,x}(z,t)$ Eq. (5) is related to the complex refractive index $\underline{n}_{\gamma S,x}(z,t)$ by the propagation equation

$$\frac{\partial}{\partial z} \mathcal{E}_{\gamma S,x}(z,t) + \frac{1}{v_g} \frac{\partial}{\partial t} \mathcal{E}_{\gamma S,x}(z,t) = -jk_0 \Delta \underline{n}_{\gamma S,x}(z,t) \mathcal{E}_{\gamma S,x}(z,t). \quad (7)$$

It is convenient to formulate the propagation of the light signals in a retarded time frame $\tau = t - z/v_g$ (functions $F_\gamma(z, t)$ transform in retarded functions $F(z, \tau)$),

$$\begin{aligned} P_{S,\times}(z, \tau) &= P_{\gamma S,\times}(z, t), & g_{S,\times}(z, \tau) &= g_{\gamma S,\times}(z, t), \\ \varphi_{S,\times}(z, \tau) &= \varphi_{\gamma S,\times}(z, t), & \Delta n_{S,\times}(z, \tau) &= \Delta n_{\gamma S,\times}(z, t). \end{aligned} \quad (8)$$

Since the retarded time τ at the SOA input ($z = 0$) coincides with the natural time t , the input pump and CW probe power dependencies as well as the input phase shifts are

$$\begin{aligned} P_S(0, \tau) &= P_{\gamma S}^{\text{in}}(\tau) = P_{\text{in}}(\tau), & P_\times(0, \tau) &= P_{\gamma \times}^{\text{in}}(\tau) = P_\times = \text{const}, \\ \varphi_{S,\times}(0, \tau) &= \varphi_{\gamma S,\times}^{\text{in}}(\tau) = 0. \end{aligned} \quad (9)$$

At the SOA output ($z = L$) we have the output pump and CW probe power dependencies as well as the output phase shifts

$$P_{S,\times}(L, \tau) = P_{\gamma S,\times}^{\text{out}}(\tau + L/v_g) = P_{S,\times}^{\text{out}}(\tau), \quad \varphi_{S,\times}(L, \tau) = \varphi_{\gamma S,\times}^{\text{out}}(\tau + L/v_g) = \varphi_{S,\times}^{\text{out}}(\tau). \quad (10)$$

We now perform the coordinate transformations (z, t) to (z, τ) in Eq. (7), separate modulus and argument of $\mathcal{E}_{S,\times}$, observe $P_{S,\times} = \mathcal{E}_{S,\times} \mathcal{E}_{S,\times}^*$, and obtain the propagation equations for the powers and the phase shifts,

$$\frac{\partial}{\partial z} P_{S,\times}(z, \tau) = g_{S,\times}(z, \tau) P_{S,\times}(z, \tau) \quad (11)$$

and

$$\frac{\partial}{\partial z} \varphi_{S,\times}(z, \tau) = -k_0 \Delta n_{S,\times}(z, \tau), \quad (12)$$

respectively. Integrating Eq. (11) over the SOA length leads to

$$P_{S,\times}(L, \tau) = P_{S,\times}(0, \tau) \exp[h_{S,\times}(\tau)], \quad h_{S,\times}(\tau) = \int_0^L g_{S,\times}(z, \tau) dz. \quad (13)$$

The power gain coefficient $g_{S,\times}(z, \tau)$ in Eq. (11) is positive and takes care of the fact that the signal power is distributed over a cross-section so that the total power is larger by the field concentration factor [23]. The highest value g_0 represents the unsaturated small-signal gain, see Eq. (6). The dimensionless integrated gain coefficient $h_{S,\times}(\tau)$ (logarithmic power gain) is also positive and determines the amplification of the respective optical signal

$$\frac{P_{S,\times}(L, \tau)}{P_{S,\times}(0, \tau)} = \exp[h_{S,\times}(\tau)]. \quad (14)$$

The integrated unsaturated gain coefficient $h_0 = g_0 L$ corresponds to the largest amplification. It is convenient to subtract h_0 from $h_{S,\times}(\tau)$ and introduce the integrated gain decrease

$$\Delta h_{S,\times}(\tau) = h_{S,\times}(\tau) - h_0 = \int_0^L [g_{S,\times}(z, \tau) - g_0] dz. \quad (15)$$

From Eq. (12) we find the solution $\Delta \varphi_{S,\times}(\tau)$ for the spatially integrated phase change of the output light with respect to the input light,

$$\Delta\varphi_{S,x}(\tau) = \varphi_{S,x}(L, \tau) - \varphi_{S,x}(0, \tau) = -k_0 L \Delta n_{S,x}(\tau), \quad \Delta n_{S,x}(\tau) = \frac{1}{L} \int_0^L \Delta n_{S,x}(z, \tau) dz. \quad (16)$$

The nonlinear output phase shift follows from Eqs. (9) and (16),

$$\varphi_{S,x}^{\text{out}}(\tau) = -k_0 \int_0^L \Delta n_{S,x}(z, \tau) dz. \quad (17)$$

In Fig. 1 we display a schematic of the dependencies listed in Eqs. (9), (10) and (16). The pump pulse $P_S^{\text{in}}(\tau)$ at the input has a symmetric shape, see red curve shown in Fig. 1(a). While propagating through the SOA, the leading edge of the pump pulse experiences a larger gain than the trailing edge, due to gain saturation. The pump pulse emerging at the SOA output, which is depicted in blue color in Fig. 1(a), has therefore an asymmetric shape with its peak power shifted to smaller τ , this has been documented in [22].

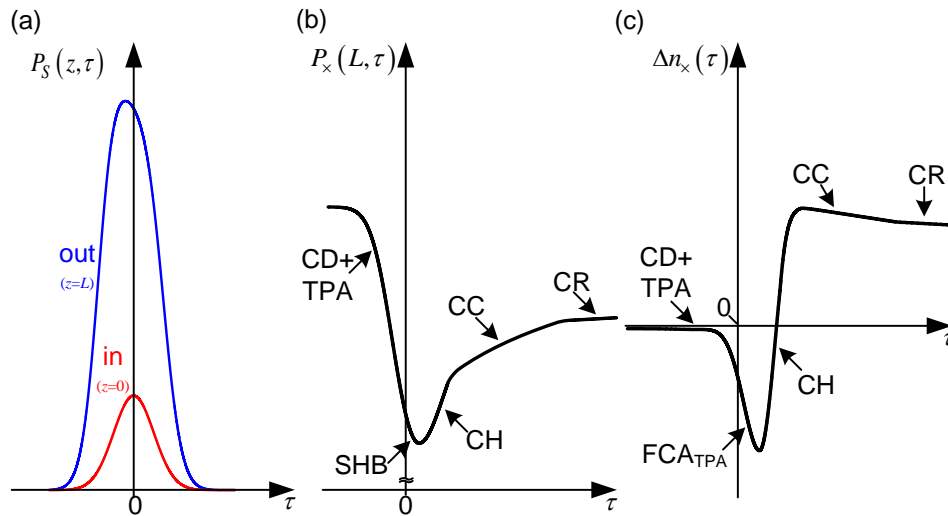


Fig. 1. Schematic input and output pump power, probe output power, and refractive index change as a function of retarded time $\tau = t - z/v_g$ (t : real time, z : propagation coordinate, v_g : group velocity). The dominant process for each time segment is marked. (a) Input pump pulse power (red line, $z = 0$) and output pump pulse power (blue line, $z = L$). (b) Probe output light power at $z = L$. (c) Refractive index change $\Delta n_x(\tau)$ according to Eq. (16), averaged over the SOA length. (CD: Carrier depletion; CH: Carrier heating; TPA: Two-photon absorption; SHB: Spectral hole burning; FCA_{TPA}: Free-carrier absorption induced by TPA; CC: Carrier cooling; CR: Carrier recovery)

The gain dynamics which results from the previously mentioned effects is probed with a weak CW input light having constant power P_x , which becomes modulated by the instantaneous gain. The power dependency of the modulated probe light $P_x(L, \tau) = P_x^{\text{out}}(\tau)$ is shown in Fig. 1(b). The gain decrease as induced by the pump pulse causes the falling slope of $P_x^{\text{out}}(\tau)$. While CD occurs over the whole pump pulse duration, only the processes dominant in each temporal segment are explicitly marked. The probe power minimum is reached *after* the (input) pump pulse maximum at $\tau = 0$, because CD, TPA and SHB are still in effect. Eventually, the SOA gain recovers, and subsequently the probe power increases towards its initial value.

The time dependency of the change in the refractive index $\Delta n_x(\tau)$ is shown in Fig. 1(c). The combined effects of CD (Section 2.1(i)) and TPA (Section 2.1(iv)) reduce the gain. However, the corresponding positive (CD) and negative changes (TPA) in the refractive

index tend to balance, resulting in a time-independent region (CD + TPA) in Fig. 1(c). The onset of SHB in Fig. 1(b) reduces the gain further, but has no effect on the refractive index change, Fig. 1(c) (Section 2.1(ii)). While all nonlinear effects in Fig. 1(b) are of first order and FCA can be neglected, the index change in Fig. 1(c) due to FCA_{TPA} decreases quadratically with the pump pulse power, so that TPA-induced free-carrier absorption (FCA_{TPA}) is responsible (Section 2.1(iv)) for the pronounced dip in the refractive index curve. During the ultrafast gain recovery (CH) the refilling of the spectral hole counteracts CD and increases the gain. Consequently, the SOA refractive index increases (Section 2.1(iii)). Once the pump signal leaves the SOA, the carrier distributions start resuming their intraband equilibrium states (CC). Finally, CR through the injection current begins and re-establishes the original carrier concentration.

2.2. Description of the analytical model

We now describe the gain and phase evolution by an analytical model in which the probe power can be considered negligible. The pump power $P_S(z, \tau)$ influences the amplification and phase shift for both pump and probe light. According to the discussion of Section 2.1(iv), a weak probe light plays an important role only for TPA processes.

As a consequence, we will treat the other processes (BF, SHB and CH) as if they had occurred in the absence of the probe, and therefore omit the subscript S for all dynamical quantities except $P_S(z, \tau)$. We emphasize that the model described below applies only to bulk SOAs.

The local modal gain coefficient $g(z, \tau)$ comprises the small signal gain coefficient g_0 and the coefficients of the gain changes $\Delta g_x(z, \tau)$ from the contributions of the processes labelled by “ x ”, i.e., $x = \{\text{BF, SHB, CH, TPA}\} [0, 1]$. By integrating the gain coefficients over the SOA length and summing up over all processes x , we obtain the logarithmic power gain $h(\tau)$, see Eqs. (13) and (15). We therefore write

$$g(z, \tau) = g_0 + \sum_x \Delta g_x(z, \tau), \quad h(\tau) = h_0 + \Delta h(\tau),$$

$$\Delta h(\tau) = \sum_x \Delta h_x(\tau), \quad \Delta h_x(\tau) = \int_0^L \Delta g_x(z, \tau) dz. \quad (18)$$

In analogy to the general relation Eq. (1), the α_x -factors associated with the above processes are denoted by

$$\alpha_x = -2k_0 \frac{\Delta n_x(z, \tau)}{\Delta g_x(z, \tau)}, \quad x = \{\text{BF, SHB, CH, TPA}\}. \quad (19)$$

The α_x -factors do not depend on time or space, because the functional dependencies of $\Delta n_x(z, \tau)$ and $\Delta g_x(z, \tau)$ are assumed to be the same. For simplicity, we neglect the coefficient Δg_{FCA} associated with the two-photon induced free-carrier absorption in our analysis and the corresponding local change $\Delta n_{FCA}(z, \tau)$ of the refractive index is derived by applying the Drude model, see Eq. (51). The total change in the refractive index $\Delta n(z, \tau)$ is given by

$$\Delta n(z, \tau) = \sum_x \Delta n_x(z, \tau) + \Delta n_{FCA}(z, \tau), \quad \Delta n_x(z, \tau) = -\frac{\alpha_x}{2k_0} \Delta g_x(z, \tau). \quad (20)$$

We substitute Eq. (20) in the right-hand side of Eq. (17) in order to determine the output phase shift of the pump field. We denote the contribution of the various processes by

$$\Delta\varphi_x(\tau) = -k_0 \int_0^L \Delta n_x(z, \tau) dz = \frac{1}{2} \alpha_x \int_0^L \Delta g_x(z, \tau) dz, \quad \Delta\varphi_{\text{FCA}}(\tau) = -k_0 \int_0^L \Delta n_{\text{FCA}}(z, \tau) dz. \quad (21)$$

Further, taking into account that $\Delta\varphi_x(\tau) = 1/2 \alpha_x \Delta h_x(\tau)$ holds, we eventually obtain

$$\varphi^{\text{out}}(\tau) = \frac{1}{2} \sum_x \alpha_x \Delta h_x(\tau) + \Delta\varphi_{\text{FCA}}(\tau). \quad (22)$$

We now start with the analytical description for band filling as developed by Agrawal and Olsson [22], and then we then include the ultrafast gain saturation as well as the TPA effect in a phenomenological fashion [21,24]. In the following, we calculate the individual gain changes $\Delta g_x(z, \tau)$ and the integrated coefficients $\Delta h_x(\tau)$ of Eq. (18) as well as the quantities $\Delta n_{\text{FCA}}(z, \tau)$ and $\Delta\varphi_{\text{FCA}}(\tau)$ related by Eq. (21).

Spatial integration techniques to account for nonlinear effects were previously described in [25] for gain recovery in SOAs, and in [26] for analyzing active and passive silicon waveguides. Such techniques are very different from the traditional discretization approach used in the context of distributed feedback semiconductor lasers [27].

2.3. Logarithmic gain

The description of the carrier dynamics in the active medium is based on rate equations [28,29].

Band filling

We assume a linear dependence of the band filling gain coefficient $g_0 + \Delta g_{\text{BF}}(z, \tau)$ on the carrier concentration $N(z, \tau)$ and write

$$\Delta g_{\text{BF}}(z, \tau) = \Gamma a [N(z, \tau) - N_{\text{st}}], \quad (23)$$

where Γ denotes the field confinement factor, a is the differential gain and N_{st} represents the unsaturated value of the carrier density [24]. In this paper we include Γ , a and N_{st} in the unsaturated (small-signal) gain g_0 , the saturation power [24] P_{sat} , and in the spontaneous carrier lifetime τ_s . We now put down a differential equation that describes the temporal evolution of band filling during a pump-probe experiment with a negligible probe light power. From the differential equation for the charge carrier concentration we find the differential equation [28] for Δg_{BF} as

$$\frac{\partial}{\partial \tau} \Delta g_{\text{BF}}(z, \tau) = - \underbrace{\left[g(z, \tau) - \frac{1}{2} \Delta g_{\text{TPA}}(z, \tau) \right]}_{\text{CD}} \frac{P_s(z, \tau)}{P_{\text{sat}} \tau_s} - \underbrace{\frac{\Delta g_{\text{BF}}(z, \tau)}{\tau_s}}_{\text{CR}}. \quad (24)$$

Band filling effects comprise carrier depletion and carrier recovery. As the unsaturated gain coefficient is always larger than the band filling gain coefficient, $\Delta g_{\text{BF}}(z, \tau) < 0$. The first term on the right-hand side of Eq. (24) is negative and therefore stands for the power gain decrease which is due to induced carrier depletion (CD). The first term also includes TPA gain. According to [28], the TPA contribution to the carrier density increase has a weight factor $1/2$, therefore we have to subtract $1/2 \Delta g_{\text{TPA}}(z, \tau)$ from the total gain $g(z, \tau)$ in Eq. (18). The second term is responsible for an increase of the gain and therefore for carrier recovery (CR) on a timescale of τ_s . For picosecond pulses, CD and CR operate on two vastly different timescales (see Section 2.1(i)) and both effects can be treated separately. Over the duration of the pump pulse, CD is instantaneous and dominates over a timescale much shorter

than τ_s , therefore CR is negligible allowing for the CR term in Eq. (24) to be set to zero. After the pump pulse has vanished, there is no more carrier depletion and now CR dominates, the first term in Eq. (24) can be neglected. We now solve Eq. (24) analytically for both cases separately. When CD dominates we use the notation $\Delta g_{\text{BF}} = \Delta g_{\text{CD}}$, and we use the notation $\Delta g_{\text{BF}} = \Delta g_{\text{CR}}$ when CR dominates. The integrated gain coefficient, $\Delta h_{\text{BF}}(\tau)$, will be accordingly denoted by $\Delta h_{\text{BF}} = \Delta h_{\text{CD}}$ and $\Delta h_{\text{BF}} = \Delta h_{\text{CR}}$.

Carrier depletion

For the case of weak to moderate pump energies, i.e., when the effects of CH, SHB and TPA on pump-induced changes in carrier density are neglected and the conditions $|\Delta g_{x \neq \text{CD}}(z, \tau)| \ll g_0 + \Delta g_{\text{CD}}(z, \tau)$ hold, the local gain coefficient $g(z, \tau)$ describes only the CD contribution $g_0 + \Delta g_{\text{CD}}(z, \tau)$ of the BF effect,

$$g(z, \tau) \approx g_0 + \Delta g_{\text{CD}}(z, \tau). \quad (25)$$

As a consequence, in determining $\Delta g_{\text{CD}}(z, \tau)$ we can approximate $P_s(z, \tau)$ by the solution $P_{\text{CD}}(z, \tau)$ of the propagation equation

$$\frac{\partial}{\partial z} P_{\text{CD}}(z, \tau) = [g_0 + \Delta g_{\text{CD}}(z, \tau)] P_{\text{CD}}(z, \tau). \quad (26)$$

Writing $P_s(z, \tau) \approx P_{\text{CD}}(z, \tau)$ the right-hand side of Eq. (24) simplifies to

$$\frac{\partial}{\partial \tau} \Delta g_{\text{CD}}(z, \tau) = -[g_0 + \Delta g_{\text{CD}}(z, \tau)] \frac{P_{\text{CD}}(z, \tau)}{P_{\text{sat}} \tau_s}. \quad (27)$$

We integrate both sides of Eq. (27) over the whole SOA length, substitute $[g_0 + \Delta g_{\text{CD}}(z, \tau)] P_{\text{CD}}(z, \tau)$ from Eq. (26), employ Eq. (13) with $P_{\text{CD}}(0, \tau) = P_{\text{in}}(\tau)$, and find a differential equation for the integrated BF gain coefficient Δh_{CD} ,

$$\frac{d}{d\tau} \Delta h_{\text{CD}}(\tau) = -\frac{\exp[h_0 + \Delta h_{\text{CD}}(\tau)] - 1}{P_{\text{sat}} \tau_s} P_{\text{in}}(\tau). \quad (28)$$

With the integrated unsaturated small-signal gain as an initial condition, $\Delta h_{\text{CD}}(-\infty) = 0$, Eq. (28) can be integrated ([22], see also Appendix B) resulting in

$$\Delta h_{\text{CD}}(\tau) = -\ln \left\{ \exp(h_0) - [\exp(h_0) - 1] \exp \left[-\int_{-\infty}^{\tau} P_{\text{in}}(\tau') d\tau' / (P_{\text{sat}} \tau_s) \right] \right\}. \quad (29)$$

For the case of Gaussian input pulses, the integral in Eq. (29) has a closed-form expression in terms of the error-function [22].

After $h_0 + \Delta h_{\text{BF}}(\tau)$ has attained its minimum, it recovers back to the unsaturated value h_0 . As the model is based on a sharp separation of CD and CR, the temporal threshold $\tau = \tau_R$ needs to be introduced. A suitable time $-\tau_R$ can be identified as the moment when the gain saturation begins. The gain reduction (in dB) up to this moment can be written as $10 \log \left\{ \exp \left[\Delta h_{\text{CD}}(-\tau_R) \right] \right\} = q$. Equation (29) allows for the determination of the time $\tau = -\tau_R$ when the gain amplification starts modifying

$$\int_{-\infty}^{-\tau_R} P_{\text{in}}(\tau) d\tau = P_{\text{sat}} \tau_s \ln \left[\frac{\exp(h_0) - 1}{\exp(h_0) - 10^{q/10}} \right]. \quad (30)$$

The energy content of the part up to $-\tau_R$ in the leading edge represents thus the largest energy for which the saturation can be neglected in the CD process. We can assume that the amplification ceases when the energy content of the final part in the trailing edge attains the amount considered negligible. For symmetric pulses, i.e., for $P_{\text{in}}(-\tau) = P_{\text{in}}(\tau)$, this happens at $\tau = +\tau_R$, due to the obvious identity $\int_{\tau_R}^{\infty} P_{\text{in}}(\tau) d\tau = \int_{-\infty}^{-\tau_R} P_{\text{in}}(\tau) d\tau$. Given a certain gain reduction q at the beginning of the saturation (at time $\tau = -\tau_R$), one can solve the resulting Eq. (30) for τ_R . This procedure is particularly useful for a Gaussian power pulse of full-width half-maximum τ_p , where the ratio τ_R/τ_p can be expressed in closed-form through the complementary error-function involving q (and other independent parameters). A practicable criterion for determining τ_R will be presented at the end of Section 3.

Carrier recovery

The differential equation for the gain recovery coefficient $\Delta g_{\text{CR}}(z, \tau)$ is found by setting the first term on the right-hand side of Eq. (24) to zero,

$$\frac{\partial}{\partial \tau} \Delta g_{\text{CR}}(z, \tau) = -\frac{\Delta g_{\text{CR}}(z, \tau)}{\tau_s}. \quad (31)$$

The CR gain dynamics for $\Delta h_{\text{BF}}(\tau)$ is obtained by integrating both sides of Eq. (31) over the SOA length and by solving the resulting differential equation for $\Delta h_{\text{CR}}(\tau)$ with the initial condition

$$\Delta h_{\text{CR}}(\tau_R) = \Delta h_{\text{CD}}(\tau_R). \quad (32)$$

The value of $\Delta h_{\text{CD}}(\tau_R)$ on the right-hand side has to be found from Eq. (29).

Overall band filling

The complete gain contribution to BF is then given by

$$\Delta h_{\text{BF}}(\tau) = \begin{cases} \Delta h_{\text{CD}}(\tau) & \tau \leq \tau_R \\ \Delta h_{\text{CD}}(\tau_R) \exp\left(-\frac{\tau - \tau_R}{\tau_s}\right) & \tau > \tau_R. \end{cases} \quad (33)$$

Our approximations lead to an analytical result, however, the time derivative of $\Delta h_{\text{BF}}(\tau)$ is no more continuous at $\tau = \tau_R$.

Spectral hole burning and carrier heating

The equations describing the intraband dynamics are stated in [29]. If intraband relaxation times are much smaller than the pulse width, the time derivative in these equations can be adiabatically eliminated, i.e., set to zero, and the local gain changes $\Delta g_{\text{SHB,CH}}(z, \tau)$ can be immediately written as [24]

$$\Delta g_{\text{SHB,CH}}(z, \tau) = -\varepsilon_{\text{SHB,CH}} \left[g(z, \tau) - \Delta g_{\text{TPA}}(z, \tau) \right] P_s(z, \tau), \quad (34)$$

with $\varepsilon_{\text{SHB,CH}}^{-1}$ being the saturation power for the respective process. Accordingly, it is the ratio of ultrafast gain compression $\Delta g_{\text{SHB,CH}}$ to the local material gain, $g - \Delta g_{\text{TPA}}$, that is proportional to the pulse power inside the SOA. The material gain itself comprises $g_0 + \Delta g_{\text{BF}}$ and the local ultrafast gain contribution $\Delta g_{\text{SHB}} + \Delta g_{\text{CH}}$ which can be calculated from Eq. (34). Denoting the total ultrafast compression coefficient by $\varepsilon = \varepsilon_{\text{SHB}} + \varepsilon_{\text{CH}}$, one can relate

$g - \Delta g_{\text{TPA}}$ to $g_0 + \Delta g_{\text{BF}}$, see the first Eq. (18). By making use of this relation in Eq. (34), one obtains

$$\Delta g_{\text{SHB,CH}}(z, \tau) = -\varepsilon_{\text{SHB,CH}} \frac{[g_0 + \Delta g_{\text{BF}}(z, \tau)] P_s(z, \tau)}{1 + \varepsilon P_s(z, \tau)}. \quad (35)$$

Equation (35) describes the ultrafast gain reduction due only to the stimulated emission that removes the “cool” carriers from the distribution. We do not consider here the carrier heating via TPA and FCA. The ultrafast processes occur simultaneously with CD, however we calculate their contributions by only considering CD, see Eq. (25). For strong pulses the amount of CD would also be affected by the strength of the ultrafast gain compression, but for moderate levels of gain compression it is sufficient to replace in Eq. (35) Δg_{BF} by Δg_{CD} and $P_s(z, \tau)$ by $P_{\text{CD}}(z, \tau)$ as defined in Eq. (26). As a consequence, $\Delta g_{\text{SHB,CH}}(z, \tau)$ can be written as

$$\Delta g_{\text{SHB,CH}}(z, \tau) = -\frac{\varepsilon_{\text{SHB,CH}}}{\varepsilon} \frac{\partial}{\partial z} \left\{ \ln [1 + \varepsilon P_{\text{CD}}(z, \tau)] \right\}. \quad (36)$$

The ultrafast compressions are obtained by integrating both sides of Eq. (36) over z from $z = 0$ to $z = L$, and by taking into account the boundary conditions

$$P_{\text{CD}}(0, \tau) = P_{\text{in}}(\tau) \text{ and } P_{\text{CD}}(L, \tau) = P_{\text{in}}(\tau) \exp[h_0 + \Delta h_{\text{CD}}(\tau)] \quad (37)$$

with the result

$$\Delta h_{\text{SHB,CH}}(\tau) = -\frac{\varepsilon_{\text{SHB,CH}}}{\varepsilon} \ln \left\{ \frac{1 + \varepsilon P_{\text{in}}(\tau) \exp[h_0 + \Delta h_{\text{CD}}(\tau)]}{1 + \varepsilon P_{\text{in}}(\tau)} \right\}. \quad (38)$$

The above results remain valid in the presence of a weak probe light. By contrast, as will be shown below, the probe light can sensibly influence the TPA-process, even when its power P_x is small.

Two-photon absorption

We describe the local gain reduction due to a degenerate TPA-process (simultaneous absorption of two identical photons) by an absorption coefficient $\Delta g_{\text{TPA}}(z, \tau)$ which is proportional to the power of the propagating light P_s and to the inverse of an effective TPA cross-section A_{TPA} [23,28], with a proportionality factor $\beta_2(\omega_s)$ called the TPA coefficient at the pump frequency ω_s :

$$\Delta g_{\text{TPA}}(z, \tau) = -\frac{\beta_2(\omega_s)}{A_{\text{TPA}}} P_s(z, \tau) \quad (\text{degenerate case}). \quad (39)$$

The area A_{TPA} is larger than the cross-section A of the active region [23], because it always includes some adjacent layers within the cladding region.

In a non-degenerate TPA-process a VB electron can reach the CB by absorbing one photon from the pump and another photon from the probe. The pump having power P_s and angular frequency ω_s is assumed to be dominantly linear polarized in the direction of the unit vector \vec{e}_s , which lies in the cross-section area of the SOA waveguide. The probe light with power P_x and angular frequency ω_x is assumed to be linearly polarized in the same plane, but along a different direction \vec{e}_x , and its contribution has to be weighted by a factor

$\beta_s(\omega_s, \vec{e}_s, \omega_x, \vec{e}_x) / \beta_2(\omega_s)$ [30,31]. The local TPA absorption coefficient $\Delta g_{\text{TPA},s}(z, \tau)$ experienced by the pump in the presence of the probe light is

$$\Delta g_{\text{TPA},s}(z, \tau) = -\frac{\beta_2(\omega_s)}{A_{\text{TPA}}} \left[P_s(z, \tau) + \frac{\beta_s(\omega_s, \vec{e}_s, \omega_x, \vec{e}_x)}{\beta_2(\omega_s)} P_x(z, \tau) \right]. \quad (40)$$

In analogy, we define the local TPA absorption coefficient $\Delta g_{\text{TPA},x}(z, \tau)$ experienced by the probe light in the presence of the pump light as

$$\Delta g_{\text{TPA},x}(z, \tau) = -\frac{\beta_2(\omega_x)}{A_{\text{TPA}}} \left[\frac{\beta_x(\omega_s, \vec{e}_s, \omega_x, \vec{e}_x)}{\beta_2(\omega_x)} P_s(z, \tau) + P_x(z, \tau) \right]. \quad (41)$$

The functions $\beta_{s,x}(\omega_s, \vec{e}_s, \omega_x, \vec{e}_x)$ depend on the relative polarization angle, $\cos^{-1}(\vec{e}_s \cdot \vec{e}_x)$, are related to each other, and become equal for $\omega_s = \omega_x$ [31]. In general, a TPA in pump-probe experiments consists of three kinds of absorption processes occurring at the same time: absorption processes of identical photon pairs from the pump and probe light, and of different photon pairs from the pump-probe coupling. For neighboring angular frequencies $\omega_s \approx \omega_x \approx \omega_0$ we introduce a new parameter r_{TPA} by the ratio

$$r_{\text{TPA}} = \frac{\beta_{s,x}(\omega_0, \vec{e}_s, \omega_0, \vec{e}_x)}{\beta_2(\omega_0)}, \quad (42)$$

write β_2 for $\beta_2(\omega_0)$ and simplify Eqs. (40) and (41) to

$$\Delta g_{\text{TPA},s}(z, \tau) = -\frac{\beta_2}{A_{\text{TPA}}} \left[P_s(z, \tau) + r_{\text{TPA}} P_x(z, \tau) \right] \quad (43)$$

and

$$\Delta g_{\text{TPA},x}(z, \tau) = -\frac{\beta_2}{A_{\text{TPA}}} \left[r_{\text{TPA}} P_s(z, \tau) + P_x(z, \tau) \right]. \quad (44)$$

The ratio r_{TPA} , hereafter called the TPA non-degeneracy factor, is positive and depends on the relative polarization angle. For semiconductors with zinc blende crystal structure $r_{\text{TPA}} = 2$ for parallel polarizations and takes a value 2-3 times smaller for orthogonal polarizations, depending on the probe frequency [31,32]. Moreover, for a weak probe light only the first term on the right-hand side of Eqs. (43) and (44) contributes, and we are left with

$$\Delta g_{\text{TPA},s}(z, \tau) = \Delta g_{\text{TPA}}(z, \tau), \quad \Delta g_{\text{TPA},x}(z, \tau) = r_{\text{TPA}} \Delta g_{\text{TPA}}(z, \tau). \quad (45)$$

Under the assumptions stated above, the local absorption coefficient from the pump in the presence of the (weak) probe light coincides with the degenerate case, Eq. (39), while the local absorption coefficient from the (weak) probe light differs from the latter by the TPA non-degeneracy factor r_{TPA} due to the pump-probe coupling. Proceeding in analogy to the fourth formula in Eq. (18) and substituting the subscript x by TPA,s and TPA,x , the integrated absorption coefficients $\Delta h_{\text{TPA},s}$ for the degenerate case and $\Delta h_{\text{TPA},x}$ for the non-degenerate case can be written with the help of Eq. (45) as

$$\Delta h_{\text{TPA},s}(\tau) = \Delta h_{\text{TPA}}(\tau), \quad \Delta h_{\text{TPA},x}(\tau) = r_{\text{TPA}} \Delta h_{\text{TPA}}(\tau). \quad (46)$$

Similarly, proceeding in analogy to Eq. (21), we find the TPA-induced phase change contributions $\Delta\varphi_{\text{TPA},S}$ for the degenerate case and $\Delta\varphi_{\text{TPA},\times}$ for the non-degenerate case:

$$\Delta\varphi_{\text{TPA},S}(\tau) = \frac{1}{2}\alpha_{\text{TPA}}\Delta h_{\text{TPA}}(\tau), \quad \Delta\varphi_{\text{TPA},\times}(\tau) = \frac{1}{2}\alpha_{\text{TPA}}r_{\text{TPA}}\Delta h_{\text{TPA}}(\tau). \quad (47)$$

The dynamical quantities in Eqs. (46) and (47), associated to the TPA-process are all expressed in terms of the contribution $\Delta h_{\text{TPA}}(\tau)$. For the calculation of this contribution according to Eqs. (18) and (39), it is necessary to integrate $P_S(z, \tau)$ over the SOA length. Since in Eq. (25) we assumed that ultrafast processes including TPA are negligible in comparison with CD, we replaced $P_S(z, \tau)$ by the solution $P_{\text{CD}}(z, \tau)$ of Eq. (26). The integration of arbitrary positive powers of $P_{\text{CD}}(z, \tau)$ is carried out in the Appendix B, yielding the coefficients $C_n(\tau)$, see Eq. (91). An explicit form of $P_{\text{CD}}(z, \tau)$ is shown in Eqs. (87) and (89). By introducing the compression coefficient

$$\varepsilon_{\text{TPA}} = \frac{\beta_2 L}{A_{\text{TPA}} h_0} \quad (48)$$

and by using the result, see Eq. (98),

$$C_1(\tau) = \frac{|\Delta h_{\text{CD}}(\tau)|}{\exp[|\Delta h_{\text{CD}}(\tau)|] - 1}, \quad (49)$$

one finds the following TPA contribution $\Delta h_{\text{TPA}}(\tau)$:

$$\Delta h_{\text{TPA}}(\tau) = -\varepsilon_{\text{TPA}} [\exp(h_0) - 1] C_1(\tau) P_{\text{in}}(\tau). \quad (50)$$

We prove in Appendix B that all coefficients $C_n(\tau)$, $n = 1, 2, \dots$ are positive and decrease with time.

2.4. FCA_{TPA} induced refractive index

In order to include the FCA_{TPA} process (as described in [16]), we assume that many of the photoexcited electrons reach the X-valley of the lowest CB by absorbing optical phonons of suitable wave vectors. Owing to the low amount of energy carried by the phonon [17], the energy of the electron remains nearly constant, while its momentum increases accordingly. Also the transit time to the X-valley expressed by the intervalley scattering time τ_0 is of order of the electron-phonon scattering time. Once arrived in the new X-valley state, the electrons can be further excited into the next higher CB by absorption of a photon. The contribution of this free-carrier absorption to the index change can be estimated on the basis of the classical oscillator model of Drude and Lorentz. By assuming the electrons moving freely in the optical field according to Newton's second law, one finds the decrease of the refractive index as given by the Drude formula [33] (elementary charge e , vacuum permittivity ε_0)

$$\Delta n_{\text{FCA}}(z, \tau) = -\frac{e^2}{2\varepsilon_0 n_0 \omega_0^2 m_{\text{FCA}}} N_{\text{FCA}}(z, \tau), \quad (51)$$

where N_{FCA} denotes the intraband density of FCA-excited electrons with effective mass m_{FCA} . Since in general $N_{\text{FCA}}(z, \tau)$ represents only a fraction K of the density $N_{\text{ex}}(z, \tau)$ of photoexcited electrons, one can write

$$N_{\text{FCA}}(z, \tau) = K N_{\text{ex}}(z, \tau - \tau_0), \quad 0 < K < 1. \quad (52)$$

An instantaneous FCA_{TPA} process in the Γ -valley where photoexcited electrons are produced needs phonon assistance and is unlikely.

In the following we consider photoexcited electrons with average lifetime τ_{ex} arising in the active region of cross-section A by TPA from the pump (power P_s , angular frequency ω_s) and probe light (power P_x , angular frequency ω_x). We describe the dynamics of these carriers by the following rate equation (\hbar is the reduced Planck constant):

$$\frac{\partial}{\partial \tau} N_{\text{ex}}(z, \tau) = -\frac{1}{2A} \left[\frac{\Delta g_{\text{TPA},s}(z, \tau) P_s(z, \tau)}{\hbar \omega_s} + \frac{\Delta g_{\text{TPA},x}(z, \tau) P_x(z, \tau)}{\hbar \omega_x} \right] - \frac{N_{\text{ex}}(z, \tau)}{\tau_{\text{ex}}}. \quad (53)$$

The first term on the right-hand side is positive and apart from the factor $1/2$ whose origin has been already explained (see Eq. (24)), represents the local density of photons absorbed per second from both, pump and probe light. The second term is negative and accounts for the loss of photoexcited electrons. By setting $P_s = P_x = 0$ one can verify that τ_{ex} is the photoexcited carrier lifetime. The double heterostructure confines all carriers in the active region, i.e., the carriers are distributed over the cross-section A . In the stationary regime $\partial N_{\text{ex}}/\partial \tau = 0$ holds, and the concentration of photoexcited electrons can be calculated from

$$N_{\text{ex}}(z, \tau) = -\frac{\tau_{\text{ex}}}{2A} \left[\frac{\Delta g_{\text{TPA},s}(z, \tau) P_s(z, \tau)}{\hbar \omega_s} + \frac{\Delta g_{\text{TPA},x}(z, \tau) P_x(z, \tau)}{\hbar \omega_x} \right]. \quad (54)$$

For closely neighbored frequencies $\omega_s \approx \omega_x \approx \omega_0$ one can substitute Eqs. (43) and (44) in Eq. (54). The contributions proportional to $P_s^2(z, \tau)$, $P_x^2(z, \tau)$ and $2r_{\text{TPA}} P_s(z, \tau) P_x(z, \tau)$ enter with the same weight and represent the three kinds of aforementioned TPA-processes, two degenerate and one non-degenerate TPA processes. For a sufficiently weak probe light, one can neglect the terms containing $P_x(z, \tau)$ such that $N_{\text{ex}}(z, \tau)$ becomes independent of the TPA non-degeneracy factor r_{TPA} ,

$$N_{\text{ex}}(z, \tau) = -\tau_{\text{ex}} \Delta g_{\text{TPA}}(z, \tau) \frac{P_s(z, \tau)}{2\hbar \omega_0 A}. \quad (55)$$

By substituting Eqs. (52), (55) and (39) into the right-hand side of the Drude formula (Eq. (51)), one gets

$$\Delta n_{\text{FCA}}(z, \tau) = -\frac{c}{\omega_0} g_0 \eta_{\text{FCA}} \varepsilon_{\text{TPA}} P_s^2(z, \tau - \tau_0), \quad \eta_{\text{FCA}} = \frac{K e^2 \tau_{\text{ex}}}{4 \varepsilon_0 \hbar c m_{\text{FCA}} \omega_0^2 n_0 A} \quad (56)$$

The dependency of Δn_{FCA} on the power squared, qualifies the FCA_{TPA} process as a fifth-order nonlinear optical effect. According to the assumption in Section 2.2 that TPA-induced free-carrier absorption has a negligible gain coefficient Δg_{FCA} , the nonlinear susceptibility $\chi^{(5)}$ [30] is real and is proportional to the product $\eta_{\text{FCA}} \varepsilon_{\text{TPA}}$. Although both factors in this product are measured in $1/W$, η_{FCA} cannot represent a compression coefficient and will be simply termed as nonlinear (optical) coefficient. The FCA_{TPA} phase contribution, Eq. (21), can be found by integration over the SOA length. As before we use the approximation from Eq. (25) to replace $P_s(z, \tau)$ by $P_{\text{CD}}(z, \tau)$, perform the integral with the methods developed in Appendix B, and obtain

$$\Delta \varphi_{\text{FCA}}(\tau) = \eta_{\text{FCA}} \varepsilon_{\text{TPA}} \left[\exp(h_0) - 1 \right]^2 C_2(\tau - \tau_0) P_{\text{in}}^2(\tau - \tau_0). \quad (57)$$

The function $C_2(\tau)$ is related to the function $C_1(\tau)$ given in Eq. (49) by the expression

$$C_2(\tau) = \frac{C_1(\tau) - [\exp(h_0) - 1]^{-1} \{ \exp[h_0 + \Delta h_{CD}(\tau)] - 1 \}}{\exp[\Delta h_{CD}(\tau)] - 1}. \quad (58)$$

As the FCA_{TPA} effect is significant, most of the electrons produced by TPA in the conduction band will have an average lifetime close to τ_0 , i.e., one also expects $\tau_{ex} \gtrsim \tau_0$. On the other hand, the validity of the steady-state solution, Eq. (55), requires τ_{ex} to be shorter than the pulse width. The large value of η_{FCA} (see Table 1) leads to a strong decrease of the refractive index. Notice that the corresponding phase shift contribution starts changing later, with a time delay τ_0 after the input pulse peak.

2.5. Summary

By definition the power amplification of a light signal is the ratio of the output to the input signal power. For a graphical representation of $P_S(0, \tau) = P_{in}(\tau)$ and $P_S(L, \tau) = P_S^{out}(\tau)$, see Fig. 1(a). Inserting Eqs. (33), (38) and (50), into the third formula in Eq. (18), one obtains

$$\Delta h_S(\tau) = \Delta h(\tau) = \Delta h_{BF}(\tau) + \Delta h_{SHB}(\tau) + \Delta h_{CH}(\tau) + \Delta h_{TPA}(\tau). \quad (59)$$

In the pump-probe experiments the overall SOA power gain

$$G(\tau) = \exp[h_x(\tau)] = \exp[h_0 + \Delta h_x(\tau)] \quad (60)$$

is always given by the probe light amplification. It is represented in Fig. 1(b) for a CW probe light. The logarithmic integrated gain $\Delta h_x(\tau)$ differs from $\Delta h_S(\tau)$ by replacing $\Delta h_{TPA,S}(\tau)$ with $\Delta h_{TPA,x}(\tau)$ (see Eq. (46)),

$$\Delta h_x(\tau) = \Delta h_{BF}(\tau) + \Delta h_{SHB}(\tau) + \Delta h_{CH}(\tau) + r_{TPA} \Delta h_{TPA}(\tau). \quad (61)$$

According to the discussion in Section 2.1(ii), we will assume that SHB does not contribute to the phase shifts $\varphi_S^{out}(\tau)$, and set the corresponding α -factor $\alpha_{SHB} = 0$. By substituting Eqs. (33), (38), (50) and (57) in Eq. (22) we find

$$\varphi_S^{out}(\tau) = \varphi^{out}(\tau) = \frac{1}{2} [\alpha_{BF} \Delta h_{BF}(\tau) + \alpha_{CH} \Delta h_{CH}(\tau) + \alpha_{TPA} \Delta h_{TPA}(\tau)] + \Delta \varphi_{FCA}(\tau). \quad (62)$$

The phase shift $\Delta \varphi_x(\tau)$ of the probe light is related to the change in the refractive index, $\Delta n_x(\tau)$, see Eq. (16), and is schematically depicted in Fig. 1(c). The quantity $\varphi_x^{out}(\tau)$ is obtained in a similar way as $\varphi_S^{out}(\tau)$ by taking into account Eq. (47),

$$\varphi_x^{out}(\tau) = \frac{1}{2} [\alpha_{BF} \Delta h_{BF}(\tau) + \alpha_{CH} \Delta h_{CH}(\tau) + r_{TPA} \alpha_{TPA} \Delta h_{TPA}(\tau)] + \Delta \varphi_{FCA}(\tau). \quad (63)$$

As an example, we calculate the gain dynamics of an SOA, driven with a Gaussian input pump pulse having 3.8 mW peak power and a full width at half maximum (FWHM) of 2.8 ps, i.e., with a pump input energy of 11.3 fJ. The parameters given in Table 1 are typical for an SOA being operated at a wavelength of 1.55 μm corresponding to a frequency of about $f_0 = \omega_0 / (2\pi) = 193.4$ THz. According to [21], the carrier lifetime τ_s lies in the range 100 ps ... 1 ns. By taking $\tau_s = 100$ ps and by choosing $P_{sat} = 50$ mW, one obtains a saturation energy $W_{sat} = P_{sat} \tau_s = 5$ pJ in agreement with the typical range of 5 ... 10 pJ reported in [22]. The α -factors are taken from [13].

We postpone the discussion of the other parameters to the end of Section 3 and first calculate the optical spectra, which we then compare to measured data.

Table 1. List of parameters used to calculate SOA gain and phase shift dynamics.
* indicates typical value for the intraband process relaxation time, though not resolved in this work.

Process	BF	CH	SHB	TPA	FCA _{TPA}
Unsaturated device gain	$h_0 = 6$	—	—	—	—
Sat. power & nonlinearity coefficient	$P_{\text{sat}} = 50 \text{ mW}$	$\varepsilon_{\text{CH}} = 0.5 \text{ W}^{-1}$	$\varepsilon_{\text{SHB}} = 0.3 \text{ W}^{-1}$	$\varepsilon_{\text{TPA}} = 0.25 \text{ W}^{-1}$	$\eta_{\text{FCA}} = 15 \text{ W}^{-1}$
TPA non-degeneracy factor	$r_{\text{TPA}} = 1$	—	—	—	—
α -parameter	$\alpha_{\text{BF}} = 3.8$	$\alpha_{\text{CH}} = 0.7$	$\alpha_{\text{SHB}} = 0$	$\alpha_{\text{TPA}} = -3$	—
Carrier lifetime & intervalley scattering time	$\tau_s = 100 \text{ ps}$	$\tau_{\text{CH}} = 600 \text{ fs}^*$	$\tau_{\text{SHB}} = 100 \text{ fs}^*$	—	$\tau_0 = 1 \text{ ps}$
Gain reduction at saturation onset	$q = 0.017 \text{ dB}$	—	—	—	—

The results of the calculated gain and phase shift dynamics are plotted in Fig. 2. They are in agreement with the measured gain and phase dynamics from pump-probe experiments [13,34,35]. Starting with the basic BF contribution, we successively add the contributions of the other processes, and are able to see how each process contributes individually to the overall gain. An important feature of the plots is the delay between the gain minimum and the refractive index maximum. This was shown experimentally and theoretically by others [13,34,35] and is also confirmed by our model.

Since the FCA_{TPA} process starts $\tau_0 = 1 \text{ ps}$ later than the TPA itself, the refractive index is stationary during this delay, see Fig. 2(c). Notice that due to the fast and ultrafast saturation effects the refractive index minimum is reached somewhat earlier than 1 ps. Neglecting Δg_{FCA} can only be compatible with moderately high TPA effects in bulk SOAs. In such cases there are fewer free-carriers arising during the FCA_{TPA} process than removed by carrier depletion. However, the absorption cross-sections calculated in [16] are in the order of the BF differential gain. This fact can satisfactorily explain the dramatic FCA_{TPA} phase-shift shown in Fig. 2(c) by simultaneously keeping the negligible free-carrier absorption stipulated in Fig. 2(b). The topic is thoroughly discussed in Appendix A.

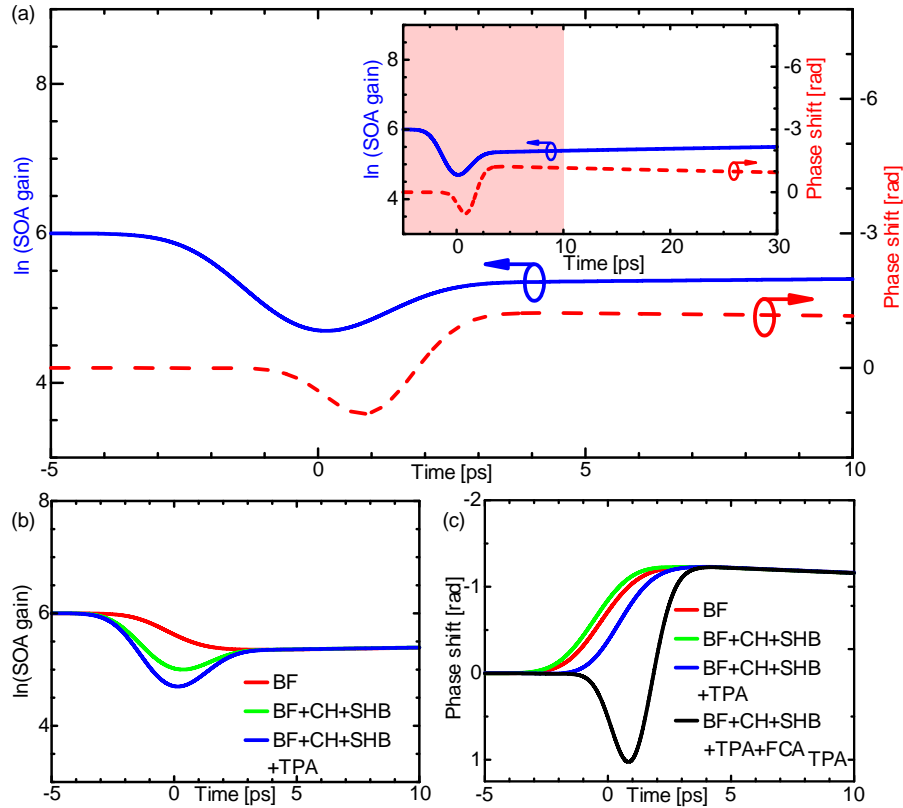


Fig. 2. Calculated time dependence of SOA gain $G = \exp(h_x)$. The origin $\tau = 0$ of the retarded time coincides with the maximum of the pump pulse $P_i(0, \tau)$, see Fig. 1. With our model we calculate $\ln(G) = h_x$ and the phase shift $\Delta\varphi_x = -k_0 L \Delta n_x$. (a) Gain and phase shift as a function of retarded time. The inset shows a blow-up. (b) Gain and (c) phase contributions of the various effects. (BF: Band filling; TPA: Two photon absorption; FCA_{TPA} : TPA-induced free-carrier absorption delayed by the intervalley scattering time $\tau_0 = 1$ ps; SHB: Spectral hole burning; CH: Carrier heating).

The advantage of using this approach is the ability to analytically model the temporal gain dynamics with the few parameters of Table 1. Most of these parameters can be derived by fitting the calculated spectrum to the measured one. The model does not require details on the geometry and on the other SOA parameters which typically are inaccessible.

3. Pump and probe light spectra at SOA output: comparison of model and measurements with experiment

The closed form expressions for the gain and phase dynamics, in which only a few constant parameters are chosen independently, allows us to derive the spectral shapes and to compare them with the experiment. Moreover, one can determine the remaining constant parameters by fitting the spectral traces and hence get a better understanding of the dynamic behavior of an SOA at the respective operation point. The model parameters discussed at the end of this section are found to be within a $\pm 10\%$ spread of their absolute extracted values.

In the following we assume that the condition $P_{in0} > P_x$ is met, and P_{in0} denotes the peak power of the pump pulse $P_{in}(\tau)$, i.e., $P_{in0} = \max[P_{in}(\tau)]$ and P_x is the CW probe light power. We also assume – as before – that the pump and CW frequencies are not too far apart. According to Eqs. (61) and (63), one needs an additional parameter, the TPA non-degeneracy factor r_{TPA} , for describing the amplification and the phase shift of the probe light. Only if

$r_{\text{TPA}} \approx 1$ holds, the propagation of a weak probe light does not influence the active medium. Since the SOA material is assumed to have a negligible dispersion, we can use the same values of the constant parameters other than r_{TPA} , for both signals.

For a comparison with the experiment, we calculate the one-sided power spectra $\Theta_{S,\times}$ for the real optical pump (subscript S) and probe (subscript \times) fields at the SOA output. Starting with the output normalized RMS electric fields $E_{\gamma S,\times}^{\text{out}}(t)$ as given by Eq. (4), we perform the Fourier transform of the real part $\Re\{E_{\gamma S,\times}^{\text{out}}(t)\}$. We then shift it from the carrier angular frequencies $\omega_{S,\times}$ to the baseband, observe a factor of $1/2$ for the one-sided transform, take the modulus square and express the resulting power spectrum versus the frequency shift $f = (\omega - \omega_{S,\times})/(2\pi)$,

$$\Theta_{S,\times}(f) = \left| \frac{1}{2} \int_{-\infty}^{\infty} \sqrt{P_{\gamma S,\times}^{\text{out}}(t)} \exp[j\varphi_{\gamma S,\times}^{\text{out}}(t)] \exp[-j(k_0 n_0 L + 2\pi f t)] dt \right|^2. \quad (64)$$

The powers and phase shifts of the output signals are obtained in terms of $\Delta h_{S,\times}(\tau)$, see Eqs. (59) and (61), and $\varphi_{S,\times}^{\text{out}}(\tau)$, see Eqs. (62) and (63). Writing

$$P^{\text{out}}(\tau) = \exp[h_0 + \Delta h_S(\tau)] P_{\text{in}}(\tau) \text{ and } P_{\times}^{\text{out}}(\tau) = \exp[h_0 + \Delta h_{\times}(\tau)] P_{\times}, \quad (65)$$

the retarded time dependencies from Eqs. (9) and (10) allow to express the optical spectra as

$$\Theta_{S,\times}(f) = \left| \frac{1}{2} \int_{-\infty}^{\infty} \sqrt{P_{S,\times}^{\text{out}}(\tau)} \exp[j\varphi_{S,\times}^{\text{out}}(\tau)] \exp(-j2\pi f \tau) d\tau \right|^2. \quad (66)$$

The calculated and measured spectra of the pulse and probe light at the SOA output are shown in Fig. 3(a) and Fig. 3(b). Mode-locked pulses with a 2.8 ps FWHM are generated at the repetition rate of 10 GHz in order to allow the complete CR between two successive pulses. Pump and probe light are injected in co-propagating direction into the SOA, utilizing a 3 dB coupler. The spectra were recorded by an optical spectrum analyzer with a resolution bandwidth of 0.1 nm, and correspond to the envelope of the oscillatory structure related to the pulse repetition rate.

Pulse spectra help investigating the dynamics of the gain and refractive index. Due to the short pulse duration of a few picoseconds, only nonlinear effects that occur while the pump is present show up in the output spectrum of the pump. Whereas, the probe senses both the ultrafast effects that occur when the pump is present and also the slower effects like CR that do not influence the pump. Hence, the temporal limitation of the injected optical power acts as a gating mechanism which allows to get insight of the dynamics at the beginning, while suppressing later effects. The full dynamics of the SOA gain and refractive index can be concluded from the probe light spectra. Although possibly significant effects such as spectral artifacts [21] and amplified spontaneous emission (ASE) were not included in the analytical model, the calculated spectra (solid black lines) resemble the measured ones (light grey lines). For instance, one observes the pronounced side lobes in the blue-shifted spectral domain of calculated and measured pump and probe spectra. The origin of this spectral region can be traced back to the FCA_{TPA} nonlinear effect – as described by the parameters η_{FCA} and τ_0 , see Fig. 3(c) and Fig. 3(d).

Both measured and simulated probe light spectra have broad and pronounced red-shifted spectral components extending beyond -200 GHz with respect to the center frequency, see Fig. 3(b). They mainly originate from CD and CH effects. Towards higher frequencies with respect to the center frequency one can notice two blue-shifted spectral regions. First, there is a blue-shifted spectral range starting closely to the carrier frequency. This can be attributed to

the slow carrier recovery process. We attribute the small blue-shifted shoulder with a peak around 100 GHz to the presence of both TPA and FCA_{TPA} nonlinear effects, Fig. 3(d).

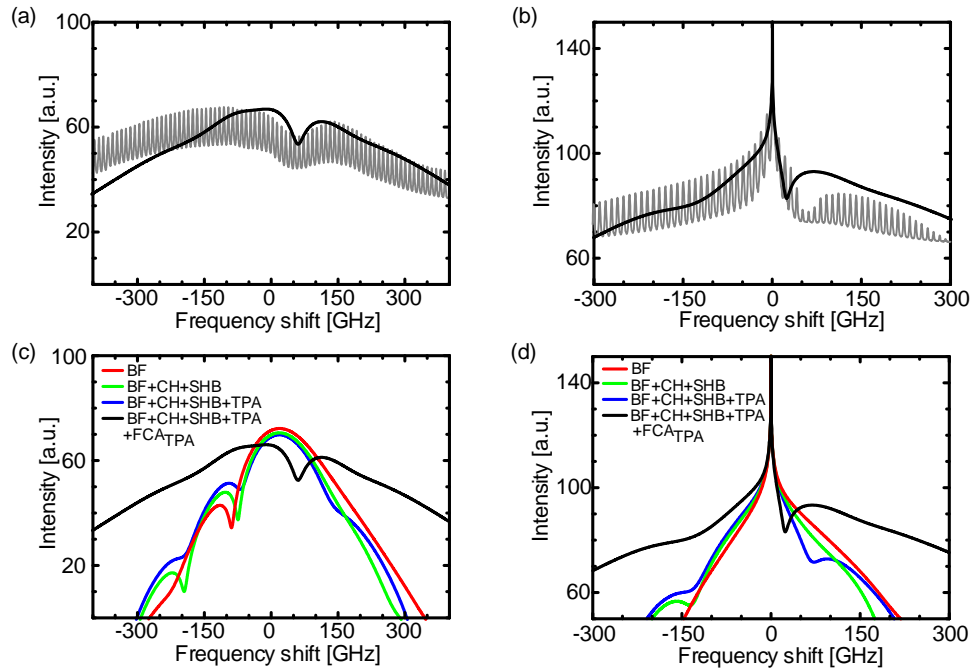


Fig. 3. Calculated spectra (log scale) using the parameters from Table 1 and comparison with measured ones. (a) Measured (light gray lines) and calculated (solid black lines) spectra after the SOA of the pump pulse and (b) measured (light gray lines) and calculated (solid black lines) spectra after the SOA of the probe light. The decomposition of the spectra is shown in (c) for the pump pulse and in (d) for the CW pulse light. (BF: Band filling; TPA: Two photon absorption; FCA_{TPA} : Free-carrier absorption induced by TPA; SHB: Spectral hole burning; CH: Carrier heating).

Other researchers have found similar spectral characteristics, particularly when experiments have been performed with short pulses of 1 ps [36] and 2 ps [37]. The discussion here has shown that the presence or absence of spectral components gives an indication for the occurrence and strength of a particular nonlinear effect. Specifically, one expects a distinct blue-shifted side-lobe far off from the center frequency in the presence of TPA and FCA_{TPA} , and a red-shifted spectral component due to CD and CH as well as a blue-shifted spectral component nearby the center frequency due to CR.

In Fig. 4 we present pump and probe spectra for different pulse input powers which allow to verify the differences in order of nonlinearity. Note the characteristic behavior of the blue sideband intensity associated with FCA_{TPA} . For $P_{in} = 7$ dBm, dip due to SHB can be seen at the input peak frequency.

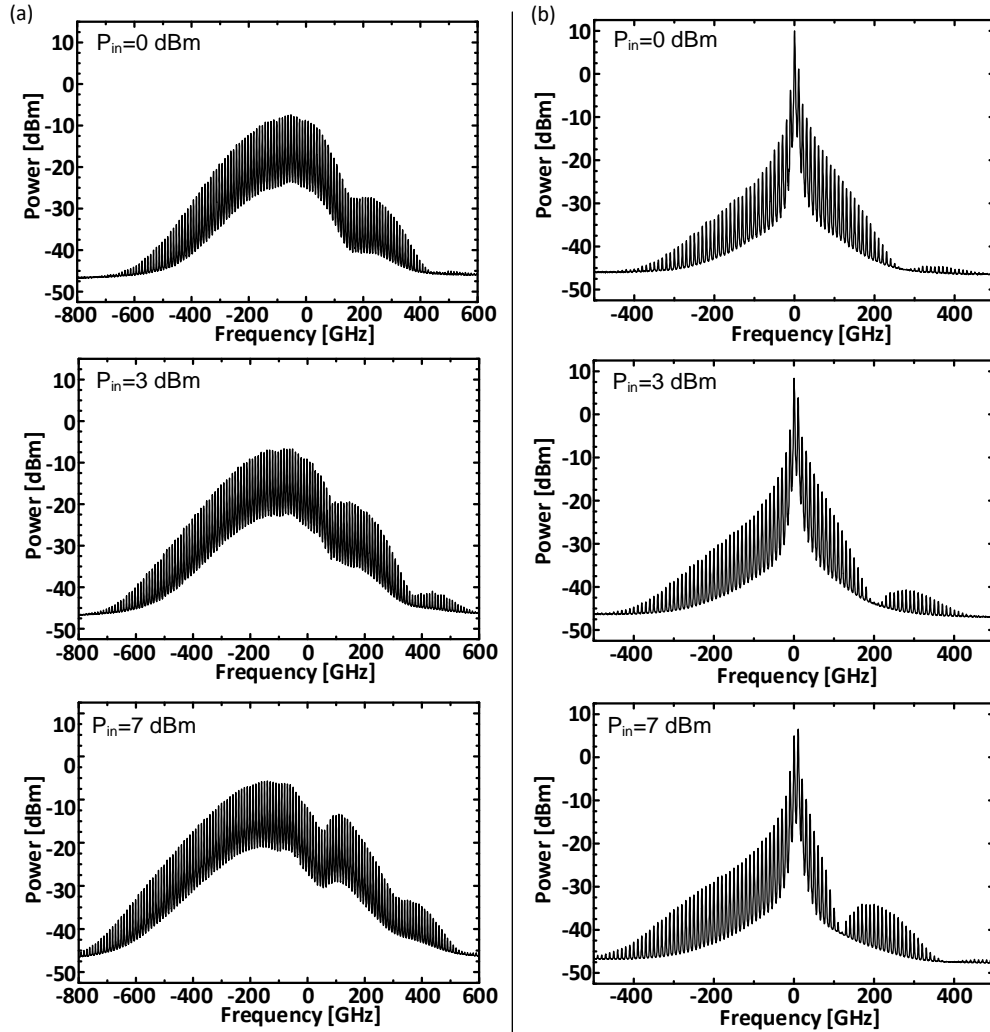


Fig. 4. Optical spectrum for $P_{in} = 0, 3, 7$ dBm; $P_{cw} = 2$ dBm; $I = 400$ mA of the (a) pump light and (b) probe light behind the SOA. The frequency origin corresponds to the input pump peak and to the probe light frequency, respectively.

The method outlined here allows to easily recognize when TPA and FCA_{TPA} play a role by just looking at the spectrum and by observing that the ultrafast decrease of the refractive index occurs during the trailing edge of the pump pulse. In addition, the method allows for an estimation of the nonlinear coefficients in a particular SOA at a certain operating point (see, e.g., Table 1). For instance, in our experiment we have employed an SOA with the structural parameters from [13]: $L = 2.6$ mm, $A = 0.225 \mu\text{m}^2$, field confinement factor $\Gamma = 0.351$ and $v_g = 8.4 \times 10^7$ m/s. Following [21], we take the TPA effective cross-section to be of the same size as the modal cross-section, $A_{TPA} = A/\Gamma$. By using Eq. (48), we estimate the nonlinear TPA coefficient β_2 from ϵ_{TPA} which is given in Table 1, and find a value of 37 cm/GW which is close to the value of 35 cm/GW reported in [21] for InGaAsP-SOAs. We also express the ultrafast compression coefficients in m^3 facilitating the comparison with the values given in literature: $\epsilon_{CH} = 3.5 \times 10^{-24} \text{m}^3$ and $\epsilon_{SHB} = 2.1 \times 10^{-24} \text{m}^3$.

We now look for the parameters q , η_{FCA} , τ_0 and r_{TPA} , which do not change the calculated optical spectra. A reduction of the gain by $q = 0.01$ dB compared to the

unsaturated gain marks the beginning of saturation and corresponds to a time $\tau_R = 3.3$ ps for a transition from CD to CR and to a ratio $14.5\text{--}15.5\text{ W}^{-1}$ of the output pulse power at τ_R , $P_S^{\text{out}}(\tau_R)$, to the peak output power, $P_S^{\text{out,peak}}$,

$$X_R = P_S^{\text{out}}(\tau_R) / P_S^{\text{out,peak}} = 4\%. \quad (67)$$

We could not see any spectral change for $q < 0.03$ dB or, equivalently, for $X_R < 9.5\%$, i.e., for transition times from CD to CR larger than 2.9 ps. The value $q = 0.017$ dB reported in Table 1 corresponds to $\tau_R = 3.1$ ps and a ratio $X_R = 6\%$.

In order to assign values to the remaining fit-parameters, a sensitivity analysis has been performed. For this purpose, we consider the relative error

$$F_{S,x}(f) = \frac{|\Theta_{S,x}^{\text{measured}}(f) - \Theta_{S,x}^{\text{calculated}}(f)|}{\Theta_{S,x}^{\text{measured}}(f)}, \quad (68)$$

and denote its averaged value over the whole measured spectrum with $\langle F_{S,x} \rangle$. We determine by calculation the changes of a single parameter leading, or corresponding to a minimum of $\langle F_{S,x} \rangle$. We then look for physical or model dependent reasons impeding the realization of this minimum. As a plausibility check, the parameter q is a useful indicator for the onset of carrier saturation. It also stands for a time τ_R , which has to be longer than the pulse duration (FWHM of the pump pulse). Approximate values for τ_0 and r_{TPA} result from their physical meanings and can be used as a first guess in the optimization algorithm. The value $\eta_{\text{FCA}} = 15\text{ W}^{-1}$ in Table 1 can be subsequently determined from the agreement of the calculated and measured spectra. The relative error averaged over the whole measured probe light spectrum $\langle F_x \rangle$ has a minimum for $q = 0.017$ dB. By keeping this value for q constant, a sensitivity analysis has been performed for the parameters η_{FCA} , τ_0 and r_{TPA} . The following ranges have been established in this way: $14.5\text{--}15.5\text{ W}^{-1}$ for η_{FCA} , $0.9\text{--}1.1$ ps for the $\Gamma \rightarrow X$ intervalley scattering time τ_0 and $0.9\text{--}1.1$ for the TPA non-degeneracy factor r_{TPA} . Recalling that $r_{\text{TPA}} = 1$ describes the TPA-process for the pump alone, we conclude that in our measurements, the probe light has no measurable effect on the active medium.

4. Selecting spectral regions to perform optical filter based wavelength conversion

The previous section has shown that nonlinear effects in an SOA lead to unique spectral traces. With our model, we can estimate their qualitative and quantitative relevance. This information is useful to judge if a particular effect is present at all, and if it is sufficiently large to be exploited in a nonlinear experiment.

There are three distinct spectral ranges which feature strong nonlinear effects. We now discuss the SOA with respect to its capability to perform all-optical signal processing by exploiting the nonlinear cross-gain modulation (XGM) and cross-phase modulation (XPM) effect.

The basic features within the phase dynamics and the spectral components as seen by a probe light are schematically depicted in Fig. 5. Both figures are derived from the plots in Fig. 2(c) and Fig. 3(b). The colors indicate three temporal regions associated with three distinct nonlinear effects as discussed in Fig. 1(c). In the previous section we have shown that the dominant nonlinear effects in the three different temporal regions yield clear spectral traces in different spectral regions. So, for instance, the blue-shifted (BS) shoulder away from the central frequency (shown in dark blue) is due to the ultrafast sharp decrease of the refractive index due to TPA and FCA_{TPA} in the first time segment. Next, the strong red-shifted (RS) spectral component (shown in red color) is mainly induced by the carrier depletion in the SOA. Finally, the spectral component close to the CW (in light blue color)

results from the carrier recovery in the active medium. Note that a fast CR process causes a broad component.

Thus, SOA nonlinear effects create new spectral components, first in the far blue, then in the red and again in the near blue spectral domain [38]. By combining an SOA with properly adjusted optical filters one can build simple and efficient all-optical wavelength converters.

A wavelength converter generating non-inverted signals is schematically depicted in Fig. 6. Using suitable red-shifted optical filters (RSOF) after an SOA, a wavelength converter can be realized. In [39], a 10 Gbit/s and a 40 Gbit/s all-optical regeneration experiment has

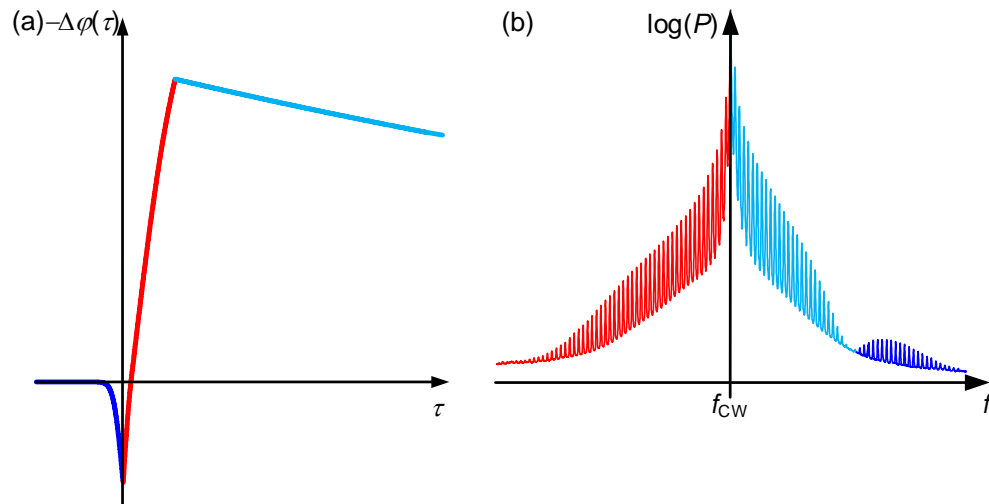


Fig. 5. Probe light phase shift and optical spectrum. (a) Phase shift dynamics and (b) corresponding induced spectral components in a measured probe light spectrum

been performed with a red-shifted optical filter offset by about 50 GHz from the center frequency. In another demonstration, the blue spectral range close to the CW carrier has been exploited for performing all-optical wavelength conversion, using blue-shifted (BSOF) optical filtering. In [40], a BSOF experiment where the filter is offset by approximately 60 GHz has been demonstrated at 40 Gbit/s.

Finally, the ultra-fast nonlinear TPA and FCA_{TPA} effects can be used. While the power in the spectral component is lowest, this spectral component is created by the fastest nonlinear effect. Since this effect does not depend on the carrier density, there is no contribution from the carrier dynamics that suffer from patterning effects. The spectral contribution due to FCA_{TPA} is very distinctive in the output probe spectrum and its presence in the spectrum is clearly recognizable. One would immediately know of the presence of the ultrafast FCA_{TPA} effects in their SOA and be able to optimize the experimental conditions in order to maximize this FCA_{TPA} contribution for their optical signal processing needs. Indeed, successful patterning free all-optical wavelength conversion at 320 Gbit/s has been demonstrated [41]. In that experiment, the filter was offset by more than 150 GHz from the center frequency, where we previously identified the dominant nonlinear TPA and FCA_{TPA} spectral component. By combining both filter types, RSOF and BSOF, a pulse reformatting optical filter (PROF) has been realized and tested with signals up to 40 Gbit/s [42,43].

The PROF works as follows: The signal after the SOA is split into two copies. One signal copy is routed through an RSOF, delayed and attenuated with respect to the second copy which passes a BSOF. The introduced delay compensates for the group delay difference between RS and BS components. Both modified signal copies, which contain only parts of the BS and RS components, are superimposed after being equalized in power and group delay such that a return-to-zero (RZ) signal at the novel wavelength will result. All-optical

wavelength conversion supported by RSOF, BSOF or PROF leads to a signal consisting of Fourier transform limited pulses.

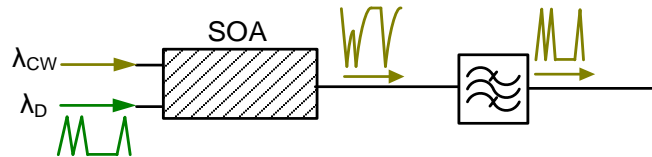


Fig. 6. Scheme of an optical filter based all-optical wavelength conversion system.

By properly offsetting the filter, each of the three spectral regions in Fig. 5(b) can be used to induce a progressive phase shift between subsequent pulses. This way RZ, vestigial-sideband (VSB) and carrier-suppressed return-to-zero (CSRZ) signals can be generated [44–46].

In this paper we have concentrated on the characterization and interpretation of the nonlinear responses of the active medium to Gaussian pulses.

5. Evidence of phase patterning effects in the spectrum

We now consider all-optical wavelength converted data signals rather than wavelength converted clock pulse-trains. The spectrum now changes, see Fig. 7. The spectrum of a 33% RZ signal at 40 Gbit/s, see Fig. 7(a), shows a central tone at the carrier frequency and two sidebands that contain the information data with tones located at multiples of the data rate. The lateral tones are accompanied by inverted spikes that are blue shifted with respect to each tone. These characteristics remain even after passing the signal through a filter for reshaping and pattern effect mitigation, e.g., a PROF as in Fig. 7(b) as well as in [45,46].

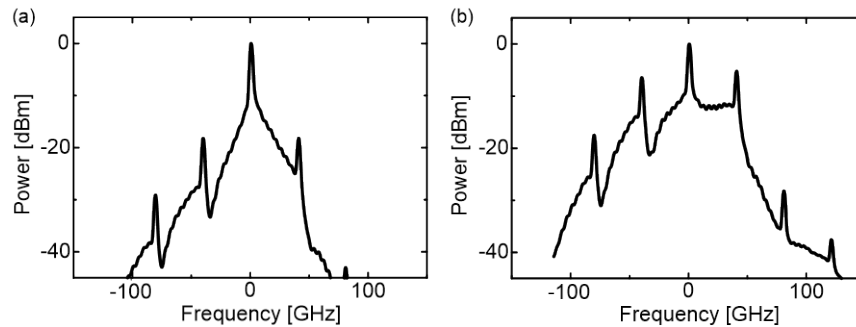


Fig. 7. Measured spectra of a 40 Gb/s wavelength converted signal. Optical spectrum (a) directly after the SOA and (b) after the PROF.

At high modulation frequencies, e.g., 40 GHz, the CR between consecutive signal pulses becomes incomplete leading thus to variations in the pulse amplitude and phase, i.e., to a patterning effect. For simplicity, we consider below only the incomplete phase restoration from bit-to-bit.

Table 2. Total signal phase change for a bit sequence of a 110100 sequence with a filter set to generate a RZ Signal and a filter offset to generate a progressive phase shifted PPS.

Sequence	1	1	0	1	0	0
Total induced phase change	$-\phi_1$	$-2\phi_1$	$-2\phi_1 + \phi_2$	$-3\phi_1 + \phi_2$	$-3\phi_1 + 2\phi_2$	$-3\phi_1 + 3\phi_2$
Total signal phase with linear phase shift PPS	PPS	$2 \cdot \text{PPS}$	$3 \cdot \text{PPS}$	$4 \cdot \text{PPS}$	$5 \cdot \text{PPS}$	$6 \cdot \text{PPS}$
	$-\phi_1$	$-2\phi_1$	$-2\phi_1 + \phi_2$	$-3\phi_1 + \phi_2$	$-3\phi_1 + 2\phi_2$	$-3\phi_1 + 3\phi_2$

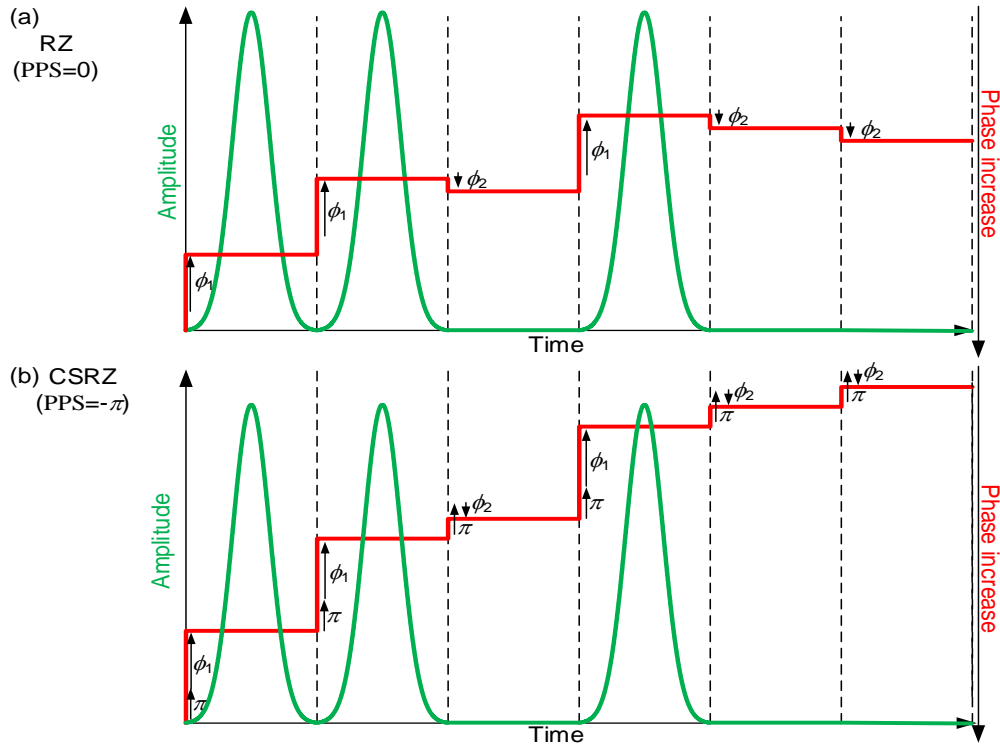


Fig. 8. Schematic description of a signal evolution. Amplitude (green line) and phase (red line) evolution of (a) an RZ signal (PPS = 0) and (b) a CSRZ signal (PPS = $-\pi$) after a filter supported wavelength conversion. A mark bit decreases the phase by ϕ_1 and a space bit increases the phase by ϕ_2 .

To demonstrate that this phase patterning leads to inverted spikes and contiguous S-shaped shoulders we propose the following model: Every mark bit entering the SOA induces a decrease of the carrier density and thus an increase of the refractive index. As a consequence, the phase of each mark bit changes by a certain value ϕ_1 , while a space bit allows for a weak phase recovery $\phi_2 < \phi_1$. So each pulse entering the SOA experiences a phase accumulated from prior pulses. For simplicity, we assume constant phase shifts ϕ_1 and ϕ_2 . They might indeed be realized for weak signals where patterning effect might add up linearly [47]. The analysis can be extended to format and wavelength converted signals. In this case a progressive phase shift PPS is added to the total phase [46]. To see the implications of phase patterning on the optical spectrum, we calculate the spectrum of an RZ and a CSRZ signal consisting of Gaussian shaped pulses with data encoded as pseudo-random bit sequence (PRBS) of $2^{11} - 1$. To each bit of the signal we then assign an accumulated phase.

Table 2 shows the signal phase assignment for an exemplary bit sequence 110100. The time evolution of the amplitude and phase shift for the bit sequence is shown in Fig. 8 for (a) RZ and (b) a signal where the filter is offset such that a CSRZ signal is generated [46]. Figure 9 shows the calculated spectra of the RZ and the CSRZ signals for $\phi_1 = \phi_2 = 0$ and for $\phi_1 = +1.875\pi$, $\phi_2 = \phi_1 / 8$.

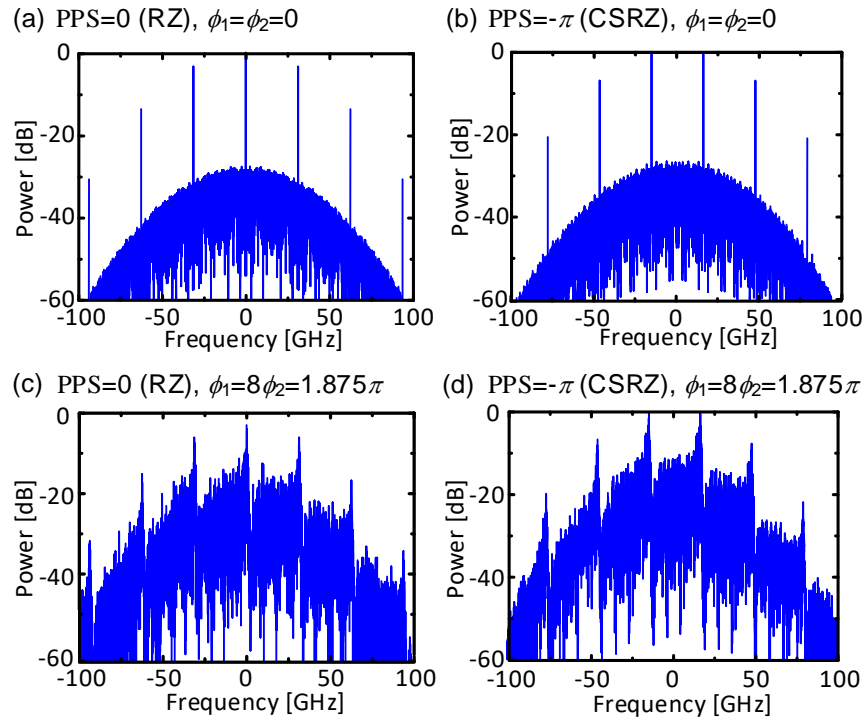


Fig. 9. Spectral traces of a phase-patterning effect. Calculated spectra for standard (a) RZ and (b) CSRZ signals and for phase patterning affect (c) RZ and (d) CSRZ signals after wavelength conversion, respectively wavelength and format conversion.

The position of the tones does not change with ϕ_1, ϕ_2 but the spectral region in-between tones shows the characteristic structure similar to the one observed in the experiment. The presence of phase patterning effect thus leaves traces in the signal spectrum.

Higher order pseudo-random bit sequences (e.g. $2^{31} - 1$) will show a slightly different output spectrum due to saturation and recovery effects. Nevertheless, since longer mark-and-space sequences contribute only to the spectral components at rather low frequencies, it will be difficult to observe the difference in the output spectrum.

6. Conclusion

We present an analytical model for the optical response of an SOA to short input pulses. By suitably adjusting the few parameters of the model we have successfully identified the nonlinear effects in the SOA from spectral traces. In particular, by comparing the calculated and measured output pump spectra, we clarified the dynamics of the refractive index during the pulse-SOA interaction. The gating mechanism of the pulse allows for the experiential to give information to conclude that the significant initial decrease of the refractive index is mainly due to an FCA_{TPA} process, which occurs as a result of an intervalley scattering. By fitting the calculated spectra for both pump pulse and CW, we determined the magnitude of the time delay and identified it with the $\Gamma \rightarrow X$ intervalley scattering time in the SOA.

More generally, we know the full dynamics of the SOA gain and refractive index. On this basis, we relate the different spectral components of the modulated probe light to the respective physical processes in SOAs. We analyze the spectrum of a converted signal and estimate the importance of three dominant effects.

When converting signals with data rates of 40 Gbit/s, the carrier density cannot recover completely within a single bit slot. The incomplete carrier recovery between subsequent marks induces a progressive increase of the refractive index inside the SOA, and a

corresponding decrease of the probe light phase, thereby leading to characteristic features in the optical spectra of a signal. This way, the spectral methods indicate the presence of patterning effects in SOA. The characteristic features observed in the spectra of the PRBS signals at high data powers are explained by assuming the constant progressive increase of the refractive index after each mark bit, and a smaller constant progressive decrease for each space bit. The regions between consecutive tones in the spectra of PRBS signals carry the information on the incomplete carrier recovery in the SOA allowing thus to see the patterning effect in the signal spectrum.

Appendix A.

The generation of TPA-induced free-carrier can occur either instantaneously (instantaneous FCA_{TPA}) by the absorption of a photon and a phonon, or via a two-stage process (delayed FCA_{TPA}), which we now describe. In the first stage, electrons are excited to the Γ -valley of the lowest conduction band (CB_1) at energies above the X-valley minima by the absorption of two photons. These photoexcited electrons are then scattered to the X-valley by short wavelength lattice phonons. The transfer to the X-valley (intervalley scattering $\Gamma \rightarrow X$) is favored by the large density of states in the X-valley as compared to the Γ -valley [16].

Both steps of this two-stage process do not occur simultaneously as there is a short delay of a few picoseconds between these two processes. Due to the specific band structure of the semiconductor material, once in the X-valley, those electrons can absorb a photon, without a phonon, to reach the next higher conduction band (CB_2).

Previous work from our group may have encountered an FCA_{TPA} process delayed by the intervalley scattering $\Gamma \rightarrow X$, because the carrier density rate equation in [13], Eq. (13), needed a correction term for carrier leakage at high carrier energies. Let W_x be the energy separation between the X-valley of CB_1 and the top of the valence band for the quaternary compound InGaAsP (see Fig. 10), and $W_{x,cl}$ be the energy separation between the aforementioned X-valley and the top of the valence band for the cladding. Then $W_x < W_{x,cl}$ holds. If by absorbing a photon of energy $\hbar\omega_0$, the condition $W_x + \hbar\omega_0 \geq W_{x,cl}$ is fulfilled, FCA-excited electrons can drift into the cladding, accounting thus for the carrier leakage.

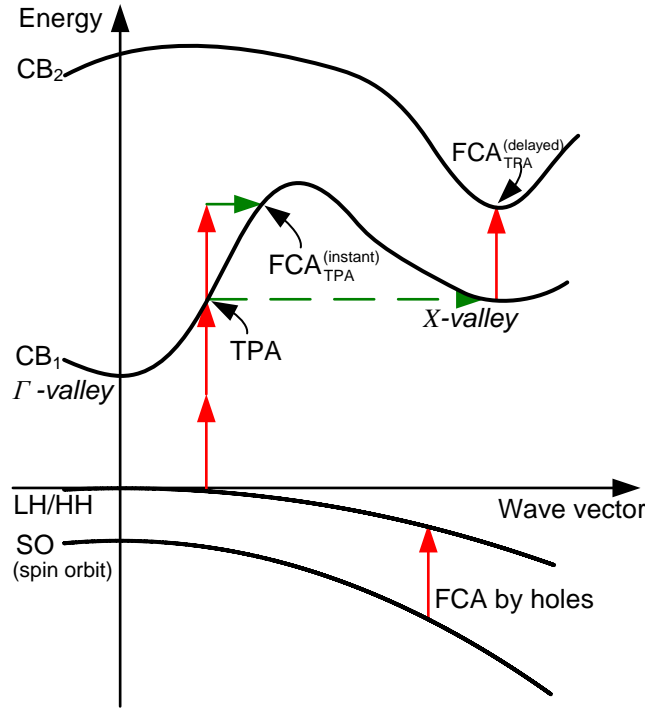


Fig. 10. Schematic of energy band diagram with TPA, intervalley scattering, FCA induced by TPA and FCA by holes. Two photons promote an electron from the light or heavy hole (LH/HH) valence band to the Γ -valley of the lowest conduction band (CB₁) at an energy above the X-valley minimum. The photoexcited electron can either remain in the Γ -valley by simultaneous absorption of one photon and one short wave vector phonon, or it can be first scattered by a long wave vector optical phonon into the X-valley and then be lifted to the next higher conduction band (CB₂) by absorbing a photon. In the process FCA by holes, an electron from spin orbit (SO) valence band absorbs a photon (without phonon assistance) and occupies a free-hole in the LH/HH valence bands. The one- and two-photon absorptions are shown by red vertical arrows, the phonon absorption by a green arrow and the intervalley scattering by a green dashed arrow.

We have tried to describe the change in the refractive index due to FCA_{TPA} by employing a minimum number of parameters, so we have neglected the FCA-coefficient $|\Delta g_{\text{FCA}}(z, \tau)|$ compared to the change $|\Delta g_{\text{BF}}(z, \tau)|$ in the BF gain,

$$|\Delta g_{\text{FCA}}(z, \tau)| \ll |\Delta g_{\text{BF}}(z, \tau)|. \quad (69)$$

By introducing the FCA cross-section σ_{FCA} , one can express the proportionality of $\Delta g_{\text{FCA}}(z, \tau)$ to the concentration $N_{\text{FCA}}(z, \tau)$ of FCA-excited electrons as

$$\Delta g_{\text{FCA}}(z, \tau) = -\sigma_{\text{FCA}} N_{\text{FCA}}(z, \tau). \quad (70)$$

A similar proportionality in terms of the concentration of depleted carriers $|N(z, \tau) - N_{\text{st}}|$ is found for the change in the BF gain coefficient, see Eq. (23). Here $N(z, \tau)$ is the total carrier density and N_{st} its unsaturated value. By substituting Eqs. (23) and (70) in the inequality Eq. (69), one can obtain an upper bound for the ratio N_{FCA} to $|N - N_{\text{st}}|$ (Γ is the confinement factor and a the BF differential gain),

$$\frac{N_{\text{FCA}}(z, \tau)}{|N(z, \tau) - N_{\text{st}}|} \ll \frac{\Gamma a}{\sigma_{\text{FCA}}}. \quad (71)$$

When the FCA cross-section and the BF differential gain are of the same order of magnitude, 10^{-20} m^2 , the right-hand side of Eq. (71) is of order one and the number of free-carriers produced by TPA cannot by far exceed the number of carriers removed by CD. As an example, let us assume for σ_{FCA} the value 10^{-20} m^2 calculated in [16], Fig. 8, for GaAs at $\lambda_0 = 1.55 \mu\text{m}$. The product Γa can be determined from the structural parameters of the employed SOA as well as from the data in Table 1, with help of the formula $\Gamma a = 2\pi\hbar c A / (W_{\text{sat}} \lambda_0)$. Substituting the numerical values for the area of the active region $A = 0.225 \mu\text{m}^2$, saturation energy $W_{\text{sat}} = P_{\text{sat}} \tau_s = 5 \text{ pJ}$ and $\sigma_{\text{FCA}} = 10^{-20} \text{ m}^2$ on the right-hand side of Eq. (71), one finds

$$\frac{N_{\text{FCA}}(z, \tau)}{|N(z, \tau) - N_{\text{st}}|} \ll 0.58. \quad (72)$$

Our SOA model is based upon the unique spectral component observed in the pump spectra and attributed to the FCA_{TPA} effect. This implies that during the pulse-SOA interaction the phase shift $\Delta\varphi_{\text{FCA}}(\tau)$ associated to FCA_{TPA} becomes much stronger than the BF phase shift $\Delta\varphi_{\text{BF}}(\tau)$. We will clarify now how such a large effect can come about with a relatively small number of FCA_{TPA} -excited carriers, see e.g., Eq. (72). We introduce the α -factors α_{FCA} and α_{BF} associated to FCA_{TPA} and BF, respectively, and write the corresponding index-change, Δn_{FCA} and Δn_{BF} , as

$$\Delta n_{\text{FCA}}(z, \tau) = -\frac{\alpha_{\text{FCA}}}{2k_0} \Delta g_{\text{FCA}}(z, \tau); \quad \Delta n_{\text{BF}}(z, \tau) = -\frac{\alpha_{\text{BF}}}{2k_0} \Delta g_{\text{BF}}(z, \tau). \quad (73)$$

By making use of the requirement Eq. (69) in Eq. (73), one can derive the inequality

$$|\Delta n_{\text{FCA}}(z, \tau)| \ll \frac{|\alpha_{\text{FCA}}|}{\alpha_{\text{BF}}} |\Delta n_{\text{BF}}(z, \tau)|. \quad (74)$$

We take into account that $\Delta n_{\text{FCA}} < 0$ and $\Delta n_{\text{BF}} > 0$ hold, multiply both sides of Eq. (74) with $(-k_0)$, integrate over the SOA length, use the definitions of the partial phase shifts, Eq. (21), and obtain

$$\Delta\varphi_{\text{FCA}}(\tau) \ll \frac{|\alpha_{\text{FCA}}|}{\alpha_{\text{BF}}} |\Delta\varphi_{\text{BF}}(\tau)|. \quad (75)$$

Both phase shifts $\Delta\varphi_{\text{FCA}}(\tau)$ and $\Delta\varphi_{\text{BF}}(\tau)$ are known in our model, and we can thus establish the retarded time $\tau = \tau_{\text{dip}}$ at which the ratio $|\Delta\varphi_{\text{FCA}}(\tau)| / |\Delta\varphi_{\text{BF}}(\tau)|$ reaches its highest value. The large effect in the FCA phase shift illustrated in Fig. 2(c) requires the following upper bound for the (negative) α -factor associated to FCA_{TPA} ,

$$\alpha_{\text{FCA}} \ll -\frac{\Delta\varphi_{\text{FCA}}(\tau_{\text{dip}})}{|\Delta\varphi_{\text{BF}}(\tau_{\text{dip}})|} \alpha_{\text{BF}}. \quad (76)$$

Substituting $\Delta\varphi_{\text{FCA}}(\tau_{\text{dip}})/|\Delta\varphi_{\text{BF}}(\tau_{\text{dip}})| = 2$ from Fig. 2(c) and $\alpha_{\text{BF}} = 3.8$ from Table 1 in Eq. (76), one finds $|\alpha_{\text{FCA}}| \gg 7.6$.

We close this appendix with the following remark: When the change in gain due to FCA_{TPA} compared with the change in the BF gain coefficient can be neglected, less than 50% free-carriers are produced by TPA than removed by BF (see Eq. (72)), while the FCA phase shift can become twice as large as the BF phase shift.

Appendix B.

In this appendix, we follow [22] to review the integration of the propagation equation for the pulse power $P_{\text{CD}}(z, \tau)$ when CR and all ultrafast processes (including TPA) are neglected. Subsequently, we develop a method for integrating arbitrary positive powers of $P_{\text{CD}}(z, \tau)$ over z .

We assume a given input pulse shape $P_{\text{in}}(\tau)$. Then the differential equation

$$\frac{\partial}{\partial z} P_{\text{CD}}(z, \tau) = g_{\text{CD}}(z, \tau) P_{\text{CD}}(z, \tau) \quad (77)$$

together with the initial condition

$$P_{\text{CD}}(0, \tau) = P_{\text{in}}(\tau) \quad (78)$$

is equivalent to the integral equation

$$P_{\text{CD}}(z, \tau) = P_{\text{in}}(\tau) \exp \left[\int_0^z g_{\text{CD}}(z', \tau) dz' \right]. \quad (79)$$

The decrease of the local gain coefficient $g_{\text{CD}}(z, \tau)$ from its small-signal value g_0 , being due to CD, is described by the rate equation (the product $P_{\text{sat}} \tau_s$ denotes the saturation energy, see [22])

$$\frac{\partial}{\partial \tau} g_{\text{CD}}(z, \tau) = -g_{\text{CD}}(z, \tau) \frac{P_{\text{CD}}(z, \tau)}{P_{\text{sat}} \tau_s}, \quad (80)$$

with the initial condition

$$g_{\text{CD}}(z, -\infty) = g_0. \quad (81)$$

In view of Eq. (79) we integrate both sides of Eqs. (80) and (81) over z , consider instead $g_{\text{CD}}(z, \tau)$ the dimensionless integral

$$h_{\text{CD}}(z, \tau) = \int_0^z g_{\text{CD}}(z', \tau) dz' \quad (82)$$

and derive the differential equation

$$\frac{\partial}{\partial \tau} h_{\text{CD}}(z, \tau) = -\frac{P_{\text{in}}(\tau) \{ \exp[h_{\text{CD}}(z, \tau)] - 1 \}}{P_{\text{sat}} \tau_s}, \quad (83)$$

with the initial condition

$$h_{\text{CD}}(z, -\infty) = g_0 z. \quad (84)$$

One can integrate the differential equation Eq. (83) by separating the variables and by noting that

$$\frac{1}{\exp[h_{\text{CD}}(z, \tau)] - 1} \frac{\partial}{\partial \tau} h_{\text{CD}}(z, \tau) = \frac{\partial}{\partial \tau} \ln \{1 - \exp[-h_{\text{CD}}(z, \tau)]\}. \quad (85)$$

By taking into account Eq. (84), the solution can be read off from

$$\ln \left\{ \frac{1 - \exp[-h_{\text{CD}}(z, \tau)]}{1 - \exp(-g_0 z)} \right\} = - \frac{1}{P_{\text{sat}} \tau_s} \int_{-\infty}^{\tau} P_{\text{in}}(\tau') d\tau'. \quad (86)$$

Equation (86) makes apparent a gain compression depending on the energy of the pulse integrated over a time interval that is much longer than the pulse width. Introducing the abbreviation

$$\mathcal{P}(\tau) = \exp \left[- \frac{1}{P_{\text{sat}} \tau_s} \int_{-\infty}^{\tau} P_{\text{in}}(\tau') d\tau' \right], \quad (87)$$

one can write the solution of Eq. (83) as

$$h_{\text{CD}}(z, \tau) = - \ln \{1 - [1 - \exp(-g_0 z)] \mathcal{P}(\tau)\}. \quad (88)$$

If one sets $z = L$ in Eq. (88) and one denotes $h_0 = g_0 L$, one can recover Eq. (29).

By substituting Eq. (88) in the right-hand side of Eq. (79), one obtains the following explicit solution of the propagation equation Eq. (77):

$$P_{\text{CD}}(z, \tau) = \frac{P_{\text{in}}(\tau)}{1 - [1 - \exp(-g_0 z)] \mathcal{P}(\tau)}. \quad (89)$$

In order to compute integrals of arbitrary positive power of P_{CD} , we introduce the time dependent, dimensionless coefficients

$$C_n(\tau) = \frac{g_0}{[\exp(h_0) - 1]^n} \int_0^L \left[\frac{P_{\text{CD}}(z, \tau)}{P_{\text{in}}(\tau)} \right]^n dz, \quad (90)$$

for $n = 1, 2, 3, \dots$. For further convenience we set $G_0 = \exp(h_0)$, $h_0 + \Delta h_{\text{CD}}(\tau) = h_{\text{CD}}(L, \tau)$, and $G_{\text{CD}}(\tau) = \exp[h_{\text{CD}}(L, \tau)]$. Then with help of Eq. (89) the coefficient $C_n(\tau)$ takes the form

$$C_n(\tau) = \frac{g_0}{(G_0 - 1)^n} \int_0^L \frac{dz}{\{1 - [1 - \exp(-g_0 z)] \mathcal{P}(\tau)\}^n}. \quad (91)$$

We provisorily suppress the time dependency and change the integration variable in Eq. (91) according to

$$u = 1 - [1 - \exp(-g_0 z)] \mathcal{P}. \quad (92)$$

We note that $u|_{z=0} = 1$ and

$$u|_{z=L} = 1 - [1 - \exp(-h_0)] \mathcal{P} = G_{\text{CD}}^{-1}, \quad (93)$$

where the last equality in Eq. (93) immediately follows from Eq. (88) with $z = L$. Using

$$g_0 dz = -\frac{du}{u-(1-\mathcal{P})} \quad (94)$$

and getting back the time dependency, one finds

$$C_n(\tau) = (G_0 - 1)^{-n} \int_{G_{\text{CD}}(\tau)}^1 \frac{du}{u^n [u - 1 + \mathcal{P}(\tau)]}. \quad (95)$$

Such integrals can be calculated by partial fraction expansion. For $n = 1$ the integral in Eq. (95) gives

$$\int \frac{du}{u(u-b)} = \frac{1}{b} \int \left(\frac{1}{u-b} - \frac{1}{u} \right) du = \frac{1}{b} \ln(1 - bu^{-1}) \quad (96)$$

with $b = 1 - \mathcal{P}$. By using the integration limits $u = 1$ and $u = G_{\text{CD}}^{-1}$ in Eq. (96), the equality on the right-hand side of Eq. (93) and the identity

$$b(G_0 - 1) = \frac{G_0}{G_{\text{CD}}} - 1, \quad (97)$$

one obtains $C_1(\tau)$ in the form announced by Eq. (49)

$$C_1(\tau) = \left[\frac{G_0}{G_{\text{CD}}(\tau)} - 1 \right]^{-1} \ln \left[\frac{G_0}{G_{\text{CD}}(\tau)} \right]. \quad (98)$$

For higher n one can derive a recurrence relation by noting the identity

$$\begin{aligned} \int \frac{du}{u^n(u-b)} &= \int \frac{u-b+b}{u^{n+1}(u-b)} du \\ &= -\frac{1}{n u^n} + b \int \frac{du}{u^{n+1}(u-b)}. \end{aligned} \quad (99)$$

One finds that the coefficients $C_{n+1}(\tau)$ and $C_n(\tau)$ are related by

$$C_{n+1}(\tau) = \left[\frac{G_0}{G_{\text{CD}}(\tau)} - 1 \right]^{-1} \left[C_n(\tau) - \frac{G_{\text{CD}}^n(\tau) - 1}{n(G_0 - 1)^n} \right]. \quad (100)$$

Equation (100) shows that all $C_n(\tau)$ can be expressed in terms of the gain contribution $\Delta h_{\text{CD}}(\tau)$ given by Eq. (29). In particular, for $n = 2$, one finds Eq. (58)

$$C_2(\tau) = \left[\frac{G_0}{G_{\text{CD}}(\tau)} - 1 \right]^{-1} \left[C_1(\tau) - \frac{G_{\text{CD}}(\tau) - 1}{G_0 - 1} \right]. \quad (101)$$

Some properties of the functions $C_n(\tau)$ are useful for recognizing their role in the gain and phase shift dynamics. From the definition Eq. (90) it follows immediately that all $C_n(\tau)$ are positive

$$C_n(\tau) > 0. \quad (102)$$

By differentiating both sides of Eq. (91) with respect to τ and by taking into account the definition of $\mathcal{P}(\tau)$, Eq. (87), one obtains

$$\frac{d}{d\tau} C_n(\tau) = -\frac{n g_0}{(G_0 - 1)^n} \frac{P_{\text{in}}(\tau)}{P_{\text{sat}} \tau_s} \mathcal{P}(\tau) \int_0^L \frac{[1 - \exp(-g_0 z)] dz}{\{1 - [1 - \exp(-g_0 z) \mathcal{P}(\tau)]\}^{n+1}}. \quad (103)$$

Obviously, the right-hand side of Eq. (103) is negative implying that $C_n(\tau)$ is a decreasing monotonic function of time with its largest value reached at $\tau = -\infty$. Substituting $\mathcal{P}(-\infty) = 1$ and $G_{\text{CD}}(-\infty) = G_0$ into Eq. (95), one can readily perform the integral over u with the result

$$C_n(-\infty) = \frac{G_0^n - 1}{n(G_0 - 1)^n}. \quad (104)$$

In particular, $C_1(-\infty) = 1$ and $C_2(-\infty) = (G_0 + 1) / [2(G_0 - 1)]$. For an unsaturated SOA gain $G_0 > 20$ dB, the right-hand side of Eq. (104) can be approximated by $1/n$.

Acknowledgment

The authors acknowledge partial funding from ETH.